ENCAPSULATING LASER-INDUCED GRAPHENE TO PRESERVE ITS ELECTRICAL AND ENHANCE ITS MECHANICAL PROPERTIES

FATEMEH BAYAT

A THESIS SUBMITTED TO THE FACULTY OF GRADUATE STUDIES
IN PARTIAL FULFILMENT OF THE REQUIREMENTS
FOR THE DEGREE OF
MASTERS OF APPLIED SCIENCE

GRADUATE PROGRAM IN ELECTRICAL ENGINEERING & COMPUTER SCIENCE
YORK UNIVERSITY
TORONTO, ONTARIO

DECEMBER 2024

Abstract

Laser-induced graphene (LIG) has emerged as a promising material in the field of printed electronics, offering excellent electrical conductivity and versatility. Its versatility stems from multiple factors: the potential for low-cost, facile, and rapid production without toxic chemicals (unlike traditional copper traces on printed circuit boards); the ability to be fabricated on various substrates; its customizable properties and its large surface area.

However, the inherent fragility of its structure poses a significant challenge, as it can be easily damaged or removed even by touching or under mechanical forces, limiting its practical applications. While a few encapsulation techniques have been explored to enhance the mechanical robustness of LIG, they often result in a significant increase in electrical resistance, diminishing its conductivity to the point where it becomes impractical for use as conductive traces in printed electronics.

In this study, we present a novel and facile approach to encapsulating LIG inscribed on a Kapton substrate while preserving the LIG's remarkable electrical properties. Through a simple and cost-effective encapsulation process involving controlled pressure application, we successfully limited the increase in resistance to just 5% of the LIG's original value. This optimal result was achieved with an applied pressure of 80 psi using a hydraulic press. The fabricated LIG exhibited

a low initial sheet resistance of approximately 2.2 Ω/sq, making it a promising candidate for applications requiring this level of resistance. Our approach offers a straightforward solution to enhancing the mechanical robustness of LIG while maintaining its desirable electrical characteristics, potentially broadening its applicability in flexible electronics and related fields.

Comprehensive characterization techniques, including Raman spectroscopy and scanning electron microscopy (SEM) were employed to investigate the structural and morphological properties of the encapsulated LIG. The results obtained from these analyses validate the efficacy of our encapsulation approach in preserving the desirable properties of LIG while enhancing its mechanical durability.

The findings of this research open up new avenues for the practical implementation of LIG in various electronic devices and applications where mechanical robustness and high conductivity are essential requirements, such as flexible and wearable electronics and flexible interconnects for conformable electronic systems. Future research endeavors can focus on further optimizing the encapsulation process, exploring alternative substrate materials, and investigating the potential integration of encapsulated LIG into diverse electronic systems and components.

Acknowledgements

First and foremost, I would like to extend my deepest gratitude to my supervisor, Dr. Simone Pisana. Thank you for the opportunity and for believing in my potential when it was still just a glimmer. Anyone would be truly lucky to have a supervisor as kind, supportive, and understanding as you. Your insights, patience, and unconditional support have not only shaped this thesis but have also significantly impacted my growth as a human being.

To my parents, who have been the greatest source of love, support, and inspiration in my life: I can't thank you enough for all the sacrifices you have made for me throughout my journey. Dad, you have provided unwavering support and made countless sacrifices, always prioritizing me. Mom, you have been a constant source of love and inspiration, and fueling my passion for science with your dedication and expertise as a chemist. I can't express enough how much I appreciate the countless ways you've helped me grow.

To my dearest partner, Matin: your love, kindness, and unwavering belief in me, even when I doubted myself, have made this journey wonderful. You have been my constant support, my home, and my family. I cannot thank you enough for always being there for me, and I am forever grateful to have you by my side.

This thesis stands as a reflection of the collective support from all these individuals. Any strengths it has are a result of their contributions, while any flaws remain my own.

Table of Contents

Abstract **ii**

Acknowledgements **iv**

Table of Contents **vi**

List of Tables **ix**

List of Figures **x**

1 Introduction **1**

1.1 Laser-Induced Graphene: Properties and Applications 1

1.2 Challenges in Mechanical Robustness of LIG 5

1.3 Encapsulation Methods for Preserving LIG Conductivity 7

1.4 Objective 11

2 Experimental Methods **13**

2.1 Fabrication of Laser-Induced Graphene 13

2.2 Measurement Techniques 17
2.3 In-situ Resistance Measurement System 20
2.4 Four-Point Probe Measurements 24
2.5 Raman Spectroscopy 26
2.6 Scanning Electron Microscopy (SEM) 29

3 Electrical Performance and Mechanical Characterization of Laser-Induced Graphene 32

3.1 Electrical Performance of As-Prepared LIG 32
3.2 Effect of Applied Force on Resistance 36
3.3 Cyclic Loading and Unloading 40
3.4 Role of Contact Resistance 43
3.5 Effect of Temperature on Resistance 44
3.6 Durability Against Moisture 47

4 Encapsulation and Mechanical Robustness 50

4.1 Encapsulation Method 50
4.2 Resistance Measurements after Encapsulation 52
4.3 Mechanical Bending Tests 57
4.4 Durability of Encapsulated LIG in Moist Environments 64

5 Structural and Morphological Characterization 69

5.1 Raman Spectroscopy Analysis 69
5.2 SEM Analysis 72

6 Conclusions **77**

6.1 Summary of Findings 77

6.2 Novel Contributions and Implications 78

6.3 Future Research Directions 79

References **80**

List of Tables

3.1 Comparison of sheet resistance values from various studies 35

3.2 Effect of rubbing on electrical resistance of LIG samples. The resistance before column indicates the initial resistance of LIG samples, and resistance after shows the resistance after rubbing with a finger. 37

3.3 Durability Against Moisture – Encapsulated LIG 48

3.4 Durability Against Moisture – Non-Encapsulated LIG 48

4.1 Effect of encapsulation pressure on electrical resistance of LIG samples after bending. The applied pressure column indicates the pressure used during encapsulation. Columns 1B, R, 2B, R, 3B, R indicate the resistance during first, second and third bends interleaved with the resistance after each bend was released, in units of Ohms. 60

4.2 Change in resistance of non-encapsulated LIG after three bending cycles with 25mm, 35mm, and 45mm bending radii 63

4.3 Resistance of encapsulated LIG before and after 24-hour water immersion 65

4.4 Resistance of non-encapsulated LIG before and after 24-hour water immersion . . . 67

List of Figures

1.1 Graphene can be wrapped up to form zero-dimensional fullerenes, rolled to form one-dimensional nanotubes, or layered to form three-dimensional graphite. [1] . . . 2

2.1 The laser process and the resulting LIG structure 14

2.2 Variation of sheet resistance with laser power from 15% (6 W) to 80% (32 W). The optimal sheet resistance was achieved at a laser power of 45% (18 W). 15

2.3 Effect of scan rate on sheet resistance at a fixed laser power of 45% (18 W). The lowest sheet resistance of 2 Ω/square was observed at a scan rate of 700 mm/min. . 16

2.4 The laser process and the resulting LIG structure 21

2.5 The laser process and the resulting LIG structure 22

3.1 Effect of finger rubbing on the structure of a laser-induced graphene (LIG) sample. The left image shows the sample before rubbing, and the right image shows the sample after rubbing. 38

3.2 The relationship between applied pressure (psi) and the percent increase in total resistance (%) of LIG samples. Each data point represents a different sample. . . . 39

3.3 Behavior of LIG resistance under repeated cycles of pressure loading and unloading. The different panels represent experiments at varying target pressures. 42

3.4 Percent change in resistance of LIG under varying pressure, comparing two-point (●) and four-point (■) measurement techniques to eliminate the possibility of contact resistance effect in the measurements. Each point represents an average of three measurements. 45

3.5 Percent change in resistance of LIG under varying pressure, in room temperature (●) and elevated 90° C temperature (■) to investigate the effect of temperature on the measurement results. 46

4.1 Percent increase in resistance of encapsulated LIG samples as a function of applied pressure. 53

4.2 Percent increase in resistance of encapsulated LIG samples as a function of applied pressure. The data is compared to LIG without encapsulation, demonstrating improved stability compared to non-encapsulated samples. 54

4.3 Correlation between applied encapsulation pressure and percentage increase in resistance, measured upon completion of three full bending cycles. 59

4.4 Experimental setup showing an encapsulated LIG sample fully immersed in water for durability testing, with contacts and wires connected to measure resistance changes. 66

4.5 Comparison of resistance changes after water exposure in encapsulated and non-encapsulated LIG samples. Error bars represent standard error (n=10 for encapsulated, n=5 for non-encapsulated, $p < 0.05$). 68

5.1 Raman spectra of our LIG samples. a) before encapsulation, b) after encapsulation with 80 psi pressure, c) after encapsulation with 780 psi pressure. The prominent peaks are the D peak near 1350 cm^{-1}, the G peak near 1600 cm^{-1}, and the 2D peak near 2700 cm^{-1}. 70

5.2 SEM images of LIG sample before encapsulation at different magnifications. 73

5.3 SEM images of LIG sample after encapsulation with 80 psi pressure at different magnifications. 74

5.4 SEM images of LIG sample after encapsulation with 780 psi pressure at different magnifications. 75

Chapter 1

Introduction

1.1 Laser-Induced Graphene: Properties and Applications

Graphene is a two-dimensional flat monolayer of carbon atoms packed into six-membered honeycomb rings. This structure serves as the building block for various carbon nanostructures: wrapped up to form zero-dimensional fullerenes, rolled to form one-dimensional nanotubes, or layered to form three-dimensional graphite [2–4], as shown in fig. 1.1. Graphene (or 2D graphite) was isolated in 2004 for the first time by Andre Geim and Konstantin Novoselov who won the Nobel prize in physics in 2010 for their significant work on graphene and its applications [5].

Graphene's exceptional properties, including its high surface area [6–8], ultra-high carrier mobility [9], high thermal conductivity [10, 11], ultra-thin thickness [12], and chemical stability [13] have made it a revolutionary material since its discovery in 2004 [8].

To further enhance these properties, graphene can be engineered into 3D porous structures,

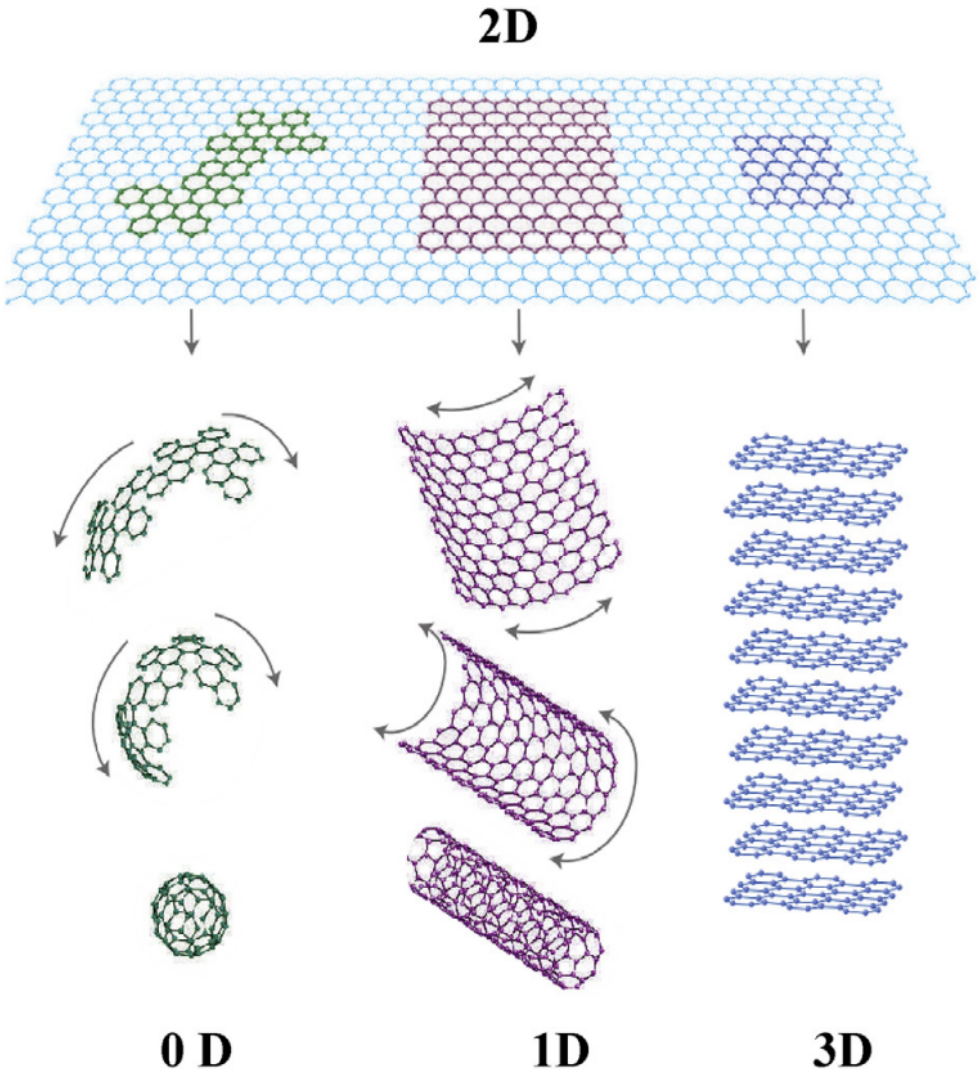

Figure 1.1: Graphene can be wrapped up to form zero-dimensional fullerenes, rolled to form one-dimensional nanotubes, or layered to form three-dimensional graphite. [1]

making it an excellent option for a wide range of applications. These include electrode materials for supercapacitors, batteries, fuel cells, water splitting cells, solar cells, flexible electronic devices, sensors, and thermal storage materials. This diverse range of applications demonstrates the versatility and significant potential of 3D graphene materials in various fields [14, 15]. However, traditional methods including hydrothermal reduction [7, 16], chemical reduction [17, 18], template-directed method [19, 20], and chemical vapor deposition (CVD) [21, 22] are complex, involving multiple steps, lengthy processes, including chemicals, and high costs. In response to these challenges, scientists in 2014 developed a simple, one-step process to directly inscribe 3D porous graphene on substrates such as polyimide using a commercial CO_2 laser. This innovation significantly streamlines the production process, eliminates the need for lengthy procedures, can be done in ambient air, avoids the use of chemicals, and reduces associated costs [23, 24]. Through this method, LIG can be patterned into various shapes, offering a straightforward approach for manufacturing printable electronics [25].

Numerous studies have investigated the influence of laser process parameters on the surface morphology, and physical, electrical, and mechanical properties of fabricated LIG. [23] By changing laser type, process atmosphere and doping and manipulating laser parameters such as wavelength, scanning speed, laser power, pulse duration, and repetition rate, researchers can fine-tune LIG's characteristics [23, 26]. Optimization of these parameters has led to the production of LIG with exceptional properties, including high porosity (340 m^2/g), remarkable thermal stability (up to 900 °C), and impressive electrical conductivity (25 S/cm) [24].

To put the electrical conductivity of LIG (25 S/cm) into perspective, it is comparable to the

conductivity of graphite perpendicular to its basal plane, which ranges from 3 S/cm to 25 S/cm (while its in-plane conductivity can range from 500 S/cm to 1700 S/cm). This value is higher than that of most semiconductors, which typically range between 10^{-8} S/cm and 10^{2} S/cm, depending on the material and conditions. However, it remains about two orders of magnitude lower than metals, which generally have conductivities exceeding 10^{4} S/cm [27] [28].

The formation of LIG through laser irradiation begins with the intense laser irradiation causing rapid local heating of the polyimide surface to extremely high temperatures. However, as the temperature continues to rise, C=O and N-C bonds subsequently break down. The remaining carbon atoms, liberated from their original molecular structure, recombine to form the graphene network. A critical step in this process is the photothermal conversion of sp3-hybridized carbon atoms to sp2-hybridized carbon atoms, which is key to the formation of the graphene structure and its resultant high electrical conductivity. The breakdown of the original polymer structure is accompanied by the release of gaseous byproducts, contributing to the porous nature of the resulting LIG. Despite the high temperatures involved in LIG formation, which would typically cause carbon to oxidize into CO_2 in ambient conditions, several factors prevent complete oxidation. The extremely rapid heating and cooling rates (approximately 10^{5} °C/s) create a localized, oxygen-deficient environment by quickly vaporizing and expelling oxygen from the reaction zone. Additionally, the decomposition of polyimide releases gases such as CO, CO_2, and hydrocarbons, which form a temporary protective atmosphere around the forming graphene. The developing porous structure of LIG may also limit oxygen diffusion to reaction sites. These combined effects allow for the formation of graphene structures rather than complete oxidation to CO_2, enabling the LIG process to occur successfully in

ambient conditions without the need for inert atmospheres. The final product of the LIG fabrication process is a black, conductive substance firmly adhered to the remaining polyimide substrate, exhibiting high electrical conductivity and a porous structure [24–26, 29–32].

This versatility and the unique properties of the resulting LIG have led to its application across a wide range of fields. In the realm of renewable energy, LIG has shown promising potential for sustainable energy conversion processes, including water treatment and fuel cell technology [6, 14]. Its unique properties make it particularly well-suited for energy storage applications, with significant advancements in the development of high-performance supercapacitors and batteries [6,14,23,33,34]. The material's exceptional sensitivity and conductivity have led to its integration in various sensing technologies [6, 35–38]. Furthermore, LIG's flexibility and ease of fabrication have opened new avenues in the field of flexible electronics [26, 39], allowing for the development of bendable and wearable devices. This wide-ranging applicability of LIG, from energy-related technologies to advanced sensing and flexible electronic systems, underscores its potential to revolutionize multiple industries and contribute to the development of more efficient and sustainable technologies.

1.2 Challenges in Mechanical Robustness of LIG

Despite the numerous advantages and potential applications of LIG, a significant challenge that impedes its widespread practical use is its inherent mechanical fragility. The structure of LIG visibly changes with a small mechanical contact. This vulnerability to mechanical stress presents a critical limitation that must be addressed to fully harness LIG's potential in real-world applications. [40, 41]

The porous nature of LIG, while beneficial for many of its applications, contributes to its

structural weakness. The laser-induced process creates a network of interconnected graphene flakes with numerous voids and defects. [37] This structure, although advantageous for applications requiring high surface area, makes the material vulnerable to fracture under mechanical forces. [42]

One primary issue is LIG's tendency to delaminate from its substrate when subjected to bending, stretching, or compressive forces. This issue can lead to performance degradation or complete failure of LIG-based devices, particularly in applications requiring flexibility or repeated mechanical movements. [43]

Furthermore, the brittle nature of LIG makes it prone to cracking and fragmentation when exposed to mechanical stress. Even relatively minor physical contacts or deformations can cause the LIG structure to break apart, disrupting its structure and electrical conductivity and diminishing its functional properties. This fragility limits LIG's potential in applications where durability and resistance to mechanical forces are critical. [44, 45]

The integration of LIG with other materials and components is also hindered by its fragile nature. Creating robust interfaces between LIG and other parts of a device or system is often challenging due to the material's fragile nature. This integration challenge impedes the development of complex, multi-material systems that could otherwise benefit from LIG's unique properties. [34]

The environmental sensitivity of LIG further compounds its mechanical robustness issues. Exposure to moisture, temperature fluctuations, or certain chemicals can alter LIG's structural durability, potentially amplifying its mechanical weaknesses over time [46]. This sensitivity raises concerns about the long-term stability and reliability of LIG-based devices, particularly in harsh or variable environments [47].

Addressing the fragile nature challenges is crucial for unlocking the full potential of LIG in various technological applications. There is a pressing need for research focused on overcoming LIG's inherent fragile nature without diminishing its beneficial characteristics such as high conductivity. [40, 43–45, 47]

The challenge of overcoming LIG's fragile nature presents an exciting opportunity for materials scientists and engineers. Overcoming this limitation could pave the way for a new generation of durable, flexible, and high-performance devices based on LIG technology. Success in this area would not only expand the practical applications of LIG but also contribute to advancing fields such as flexible electronics, energy storage, and sensing technologies.

1.3 Encapsulation Methods for Preserving LIG Conductivity

To address the challenges mentioned in the previous section, researchers have explored various encapsulation methods aimed at improving the mechanical robustness of LIG while maintaining its essential conductive properties.

Existing encapsulation approaches mainly include protective coatings [43], substrate engineering or surface treatments to improve adhesion [48, 49], optimizing the laser-induced graphene formation process to create more mechanically stable structures [50], and developing composite materials that incorporate LIG [25, 40, 43, 44].

Protective coatings involve applying a thin layer of material over the LIG surface to shield it from environmental factors. Common materials used for this purpose include polymers, such as polydimethylsiloxane (PDMS) or parylene, which offer flexibility and chemical resistance. While

effective in providing a barrier against moisture and chemicals, these coatings must be carefully selected and applied to avoid interfering with the LIG's electrical properties. For instance, the LIG has a sheet resistance of 0.13 $k\Omega/square$. This increases to 0.33 $k\Omega/square$ when coated with duct tape, 0.43 $k\Omega/square$ with low-density polyethylene (LDPE), 0.48 $k\Omega/square$ with high-density polyethylene (HDPE), 0.97 $k\Omega/square$ with the inner layer of a band-aid, and 1.79 $k\Omega/square$ with polyurethane. [43].

Composite integration represents another promising approach, wherein LIG is incorporated into a matrix material to form a composite structure. This method can enhance the overall mechanical strength of the material while potentially leveraging the properties of both the LIG and the matrix. For instance, researchers have explored the integration of LIG with epoxy resins or thermoplastic polymers to create conductive composites with improved durability. The challenge lies in achieving a balance between protection and maintaining the accessibility of the conductive LIG network. The electrical conductivity of LIG composites can vary significantly depending on the matrix material used. For example, while LIG has a sheet resistance of 0.13 $k\Omega/square$, compositing it with different materials generally results in increased resistance. For instance, a duct tape/LIG/LDPE composite shows a sheet resistance of 0.47 $k\Omega/square$, while an LDPE/LIG/HDPE structure yields 0.47 $k\Omega/square$ as well. More intricate combinations, such as LDPE/LIG/cheesecloth or LDPE/LIG/kimwipe, result in sheet resistances of 0.57 $k\Omega/square$ and 0.68 $k\Omega/square$, respectively. [25, 40, 43, 44]

Substrate engineering focuses on optimizing the interface between the LIG and its underlying substrate. This can involve exploring alternative substrate materials that offer better adhesion to

LIG or modifying existing substrates through surface treatments. For example, plasma treatment of polyimide substrates prior to LIG formation has been shown to enhance the bonding between the graphene and the substrate, potentially improving long-term stability. Recent studies have demonstrated that substrate engineering can significantly enhance the electrical and mechanical properties of LIG without compromising its conductivity. For example, increasing the wettability of polyimide substrates through localized Argon cold plasma treatment has been shown to improve the crystallinity of LIG by 21%, leading to a 51.13% increase in electrical conductivity. This improvement is attributed to the enhanced surface energy, which facilitates the diffusion of graphene nuclei, promoting better crystalline growth [48]. Similarly, researchers have enhanced LIG performance on CPI (colored polyimide) film surfaces by initially rendering them hydrophilic through oxygen plasma treatment and applying AuNPs (gold nanoparticles) solution before laser processing, resulting in Polyimide-based Au-LIG. Although the study highlights enhancements in electrochemical performance and triboelectric properties of Au-C-LIG on CPI surfaces—such as increases in surface potential and work function from 4.70 eV to 4.94 eV and exceptional sensor sensitivities of 27.56 kPa^{-1} (0–3 kPa), 6.97 kPa^{-1} (3–7 kPa), and 0.65 kPa^{-1} (7–25 kPa), it does not investigate the specific effects of these modifications on electrical conductivity [49].

Additionally, researchers have investigated modifications to the LIG formation process itself to create more mechanically stable structures. This includes optimizing laser parameters, such as power and scan speed, to produce denser and more interconnected graphene networks that exhibit improved resilience to mechanical stresses. By optimizing laser scan speed and frequency, researchers have achieved more interconnected and dense graphene networks, with needle-like structures exhibiting a

capacitance as low as 268 $\mu F/cm$, four times higher capacitance than sheet-like structures, while maintaining structural integrity and resilience [50].

While these encapsulation approaches offer various benefits, each comes with its own set of drawbacks. Some methods involve complicated steps, such as integration of LIG into composite materials, which can be time-consuming and potentially affect scalability [25, 40, 43, 44]. Others, like certain substrate engineering techniques (e.g., plasma treatment and AuNPs application) are costly and diminishing scalability in the result [48, 49]. Additionally, some approaches, such as optimizing laser parameters for more stable LIG structures, do not cause much improvement in the fragile nature of LIG [50]. The approached that include using a protective layer, increase the electrical conductivity significantly [43]. These limitations highlight the ongoing challenge of finding a balance between enhancing LIG's mechanical robustness and maintaining its essential conductive properties while keeping production processes practical, simple, and cost-effective.

Building upon these existing approaches, this thesis proposes a novel encapsulation method for LIG fabricated on polyimide substrates. The proposed technique involves encapsulating the LIG structure with an additional layer of polyimide using a hydraulic press. This approach aims to leverage the encapsulating layer to create a seamless, protected conductive structure. The use of polyimide as the encapsulating layer allows for precise control over the encapsulation process and creating a uniform protective layer that minimizes the impact on the LIG's electrical properties.

This research will explore the optimal parameters for the hydraulic press encapsulation process, including pressure and temperature. Additionally, the study will investigate the effects of this encapsulation method on the LIG's electrical conductivity, mechanical durability, and resistance to

moisture as an environmental factor.

By developing this encapsulation technique, we aim to contribute to the broader goal of enhancing the durability and reliability of LIG-based devices and structures. The successful implementation of this method could pave the way for more robust LIG applications in areas such as flexible electronics and sensors, where long-term stability under varying environmental conditions is crucial.

1.4 Objective

The primary aim of this research is to develop a novel, simple, and cost-effective method for encapsulating laser-induced graphene (LIG) that enhances its mechanical robustness while preserving its exceptional electrical properties. Specifically, this study seeks to achieve the following objectives:

- Design and implement a facile encapsulation technique for LIG using an additional layer of polyimide and a hydraulic press, aiming to create a consistent protective structure, addressed in Section 4.1 (Encapsulation Method).
- Optimize the encapsulation process parameters, including applied pressure and temperature, to achieve the best balance between mechanical protection and electrical conductivity preservation, discussed in Section 4.2 (Conductivity Measurements after Encapsulation) and partially in Section 4.3 (Mechanical Bending Tests).
- Evaluate the effectiveness of the encapsulation method in maintaining LIG's electrical conductivity, demonstrating significant improvement over the current state of the art, covered in Section 4.2 (Conductivity Measurements after Encapsulation).

- Assess the bending durability of the encapsulated LIG under various bending radii, addressed in Section 4.3 (Mechanical Bending Tests).

- Characterize the structural and morphological properties of the encapsulated LIG using techniques such as Raman spectroscopy and scanning electron microscopy (SEM), detailed in Section 5.1 (Raman Spectroscopy Analysis), and Section 5.2 (SEM Analysis).

- Compare the performance of this novel encapsulation method with existing approaches in terms of simplicity, cost-effectiveness, and preservation of LIG's desirable properties, discussed in Section 6 (Discussion and Conclusions).

By achieving these objectives, this research aims to address the current limitations in LIG technology, particularly its inherent fragility, and contribute to advancing the practical implementation of LIG in various electronic devices and applications.

Chapter 2

Experimental Methods

2.1 Fabrication of Laser-Induced Graphene

The fabrication of LIG on Kapton (Polyimide) substrates represents a significant advancement in the field of conductive materials synthesis. The primary substrate used in this study is a flexible sheet of Kapton, consisting of two layers of 125 μm thickness each, stacked together to form a combined thickness of 250 μm. The laser scribing process was performed using a CO_2 laser cutter device (Hydra 16A) manufactured by Hyrel 3D (Atlanta, GA), with a maximum power output of 40 W. The laser was employed to inscribe rectangles measuring 36 mm in length and 2 mm in width onto the polyimide sheets, utilizing vector and raster modes for length and width, respectively. Additionally, a spiral mode was implemented for fabricating the rectangles, offering versatility in the patterning process. Key laser parameters included a wavelength of 10.6 μm, laser spot size of 400 μm, focal distance of 8 mm, laser power at 45% of 40 W (18 W), pulse spacing of 1000 dots

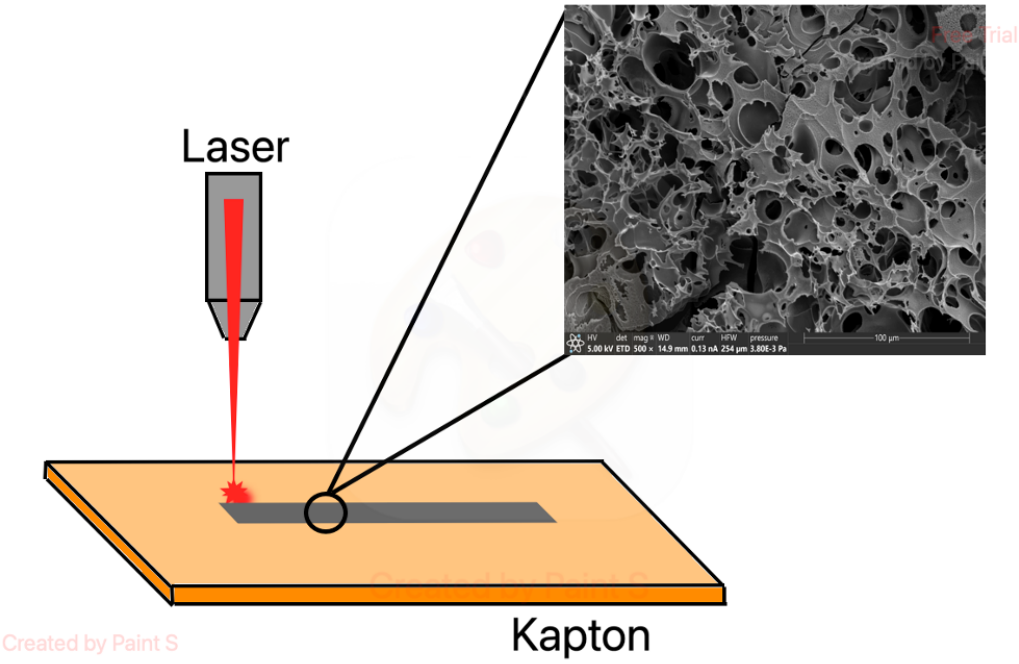

Figure 2.1: The laser process and the resulting LIG structure

per inch (DPI), and a scan rate of 700 mm/min. The temporal spacing between laser pulses was calculated to be approximately 2.178 milliseconds. All laser scribing was conducted under ambient conditions, demonstrating the process's simplicity and potential for scalability. The laser process and the resulting LIG structure is shown in Fig. 2.1.

To optimize the LIG fabrication process, we employed a systematic approach to explore and refine the two critical process parameters: laser power and scan rate. Using the G-code designed for the Hyrel laser system [30], we began by varying the laser power from 15% (6 W) to 80% (32 W) in 5% increments. The results, as shown in Figure 2.2, revealed that a power setting of 45% (18 W) produced the most favorable outcomes in terms of uniformity and quality of the LIG. Subsequently, we fixed the laser power at 45% and systematically varied the scan rate from 200 mm/min to

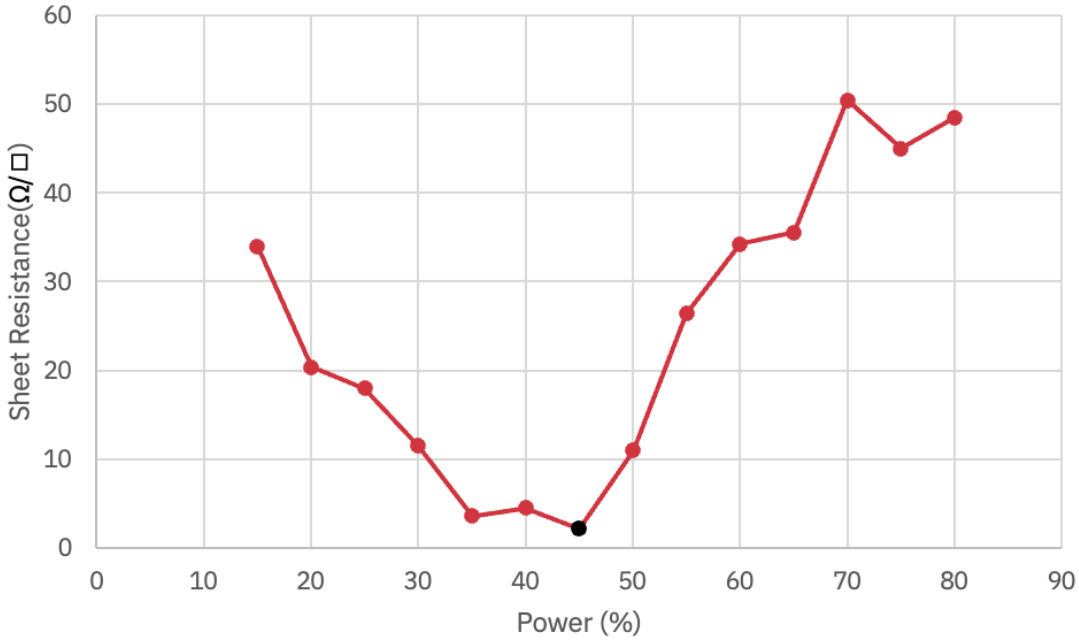

Figure 2.2: Variation of sheet resistance with laser power from 15% (6 W) to 80% (32 W). The optimal sheet resistance was achieved at a laser power of 45% (18 W).

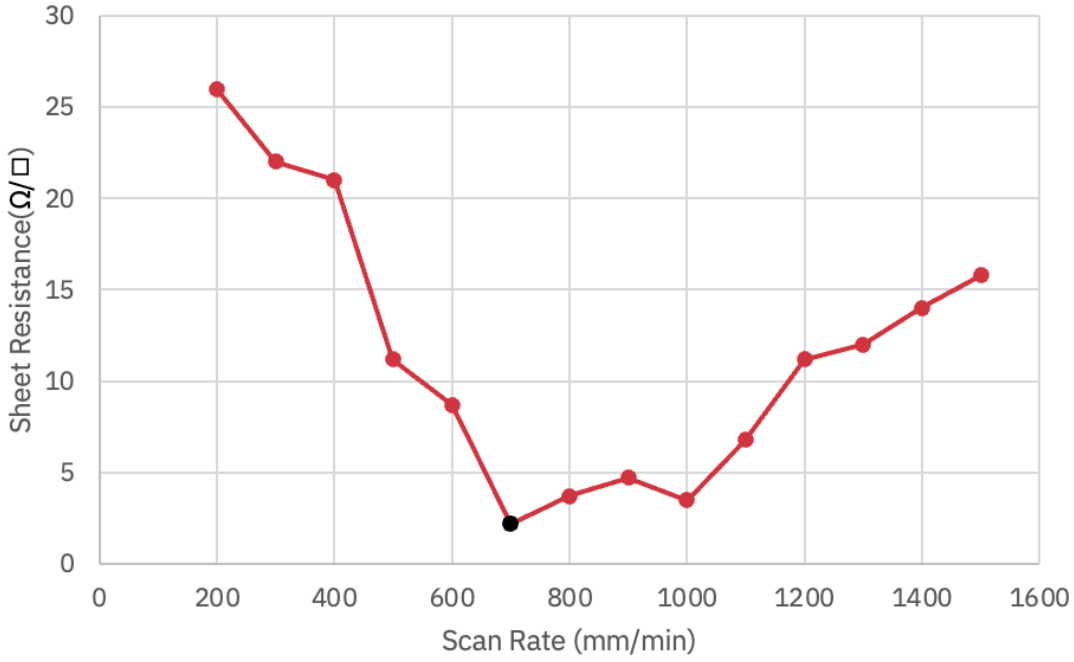

Figure 2.3: Effect of scan rate on sheet resistance at a fixed laser power of 45% (18 W). The lowest sheet resistance of 2 Ω/square was observed at a scan rate of 700 mm/min.

1500 mm/min to identify the optimal rate. As shown in Figure 2.3, this process revealed that a scan rate of 700 mm/min yielded the lowest sheet resistance, achieving values as low as 2 Ω/square. By independently varying and analyzing these parameters, we ensured a comprehensive optimization, enabling the fabrication of high-quality LIG with exceptional electrical properties. However, we may not have found a global minimum, as the parameters were changed one at a time during the optimization process.

2.2 Measurement Techniques

A diverse array of measurement techniques was employed to comprehensively characterize the properties and performance of LIG before and after encapsulation. These techniques provided crucial insights into the electrical, structural, and morphological properties of the LIG, allowing us to assess the effectiveness of our encapsulation method.

Resistance Change Measurements: To evaluate the impact of encapsulation on the electrical properties of LIG, we designed a custom *in-situ* measurement setup. This innovative approach allowed us to monitor the resistance changes in real-time while the pressure was applied using the hydraulic press. Due to the limitations of our hydraulic press, which measures pressure in psi and tons, accurately maintaining pressures below 80 psi was challenging. Although the load cell precisely indicated force in kilograms, manual adjustments of the press handle to achieve consistently lower pressure than 80 psi were difficult. By continuously measuring the resistance during the encapsulation process, we could observe how different levels of applied pressure affected the electrical conductivity of the LIG. This setup provided valuable data on the relationship between

applied pressure and the preservation of LIG's conductive properties, enabling us to optimize the encapsulation process.

During this study, two methods were employed to measure the sheet resistance of LIG. The first method utilized a four-point probe system, which was used to measure the sheet resistance of the as-fabricated LIG samples. In this method, the sample was placed under the Ossila four-point probe, which applied a constant current through the outer probes while measuring the voltage drop across the inner probes. The second method involved using a digital multimeter to measure the resistance of the samples after fabrication and encapsulation. The measured resistance was then converted to sheet resistance using the formula:

$$R_s = R \cdot \frac{W}{L}$$

where R_s is the sheet resistance in ohms per square, R is the resistance in ohms, W is the width of the sample, and L is its length.

The width (W) and length (L) of the LIG samples were measured using an optical microscope equipped with a micrometer scale, yielding precise dimensions of $W = 2\,\text{mm}$ and $L = 36\,\text{mm}$ (replace X and Y with actual values). These dimensions were used in the formula $R_s = R \cdot W/L$ to calculate the sheet resistance. The correction factor refers to the direct application of these measured dimensions to ensure accurate calculations, accounting for potential alignment or geometric inconsistencies. To validate the accuracy of these calculations, the measured resistance values were cross-verified with those obtained using the four-point probe system. This complementary approach provided robust and reliable characterization of the sheet resistance, which was critical for

evaluating the electrical properties of LIG under varying conditions.

Raman Spectroscopy: Raman spectroscopy was utilized to investigate the structural characteristics of the LIG at different stages of the encapsulation process. We analyzed three distinct samples: unencapsulated LIG, LIG encapsulated at 80 psi of pressure, and LIG encapsulated at 800 psi of pressure. This comparative approach allowed us to examine how varying levels of applied pressure during encapsulation affected the graphene structure. The Raman spectra provided crucial information about the quality of the graphene, the presence of defects, and any structural changes induced by the encapsulation process and pressure. This analysis was instrumental in understanding how our encapsulation method impacted the fundamental structure of the LIG.

Scanning Electron Microscopy (SEM): SEM imaging was employed to examine the morphological features of the LIG samples at high resolution. We analyzed three key samples: unencapsulated LIG, LIG encapsulated with 100 kg of pressure, and LIG encapsulated with 1000 kg of pressure. These images allowed us to visualize the surface structure and porosity of the LIG, and how these features were affected by different levels of encapsulation pressure. The SEM analysis provided valuable insights into the physical changes occurring in the LIG structure during the encapsulation process, helping us to correlate these morphological changes with the observed electrical and structural properties.

By combining these measurement techniques, we were able to build a comprehensive understanding of how our encapsulation method affected the various properties of LIG. This approach allowed us to optimize the encapsulation process, balancing the enhancement of mechanical robustness with the preservation of LIG's desirable electrical and structural properties. The insights gained from

these measurements were instrumental in evaluating the effectiveness and potential applications of our novel encapsulation technique.

2.3 In-situ Resistance Measurement System

To accurately assess the impact of mechanical forces on the electrical properties of LIG during the encapsulation process, we designed a custom-designed in-situ resistance measurement system. This set up is shown in fig. 2.4. This innovative setup allows for real-time monitoring of LIG's electrical resistance as varying levels of pressure are applied using a hydraulic press. The system consists of several key components working together to provide data on the relationship between applied pressure and electrical resistance. At the heart of the setup is the LIG sample, carefully prepared to ensure consistent and reliable measurements. Two contact wires are attached to the LIG sample using silver paint contacts, as shown in fig. 2.5. Silver paint was chosen as the contact material because it provides a low-resistance connection that minimizes interference with the overall resistance of the LIG sample, ensuring more accurate measurements, as shown in Fig. 4. This aspect of the setup will be further validated in section 3.3, demonstrating that the contact resistance is negligible compared to the resistance of the LIG itself.

These contact wires are connected to a high-precision digital multimeter (OWON XDM2041), as shown in fig. 2.4, which continuously measures and records the electrical resistance of the LIG sample. The multimeter's integration into the system allows for accurate and real-time tracking of resistance changes as the sample undergoes compression.

A key innovation in this setup is the incorporation of a force load cell placed directly on

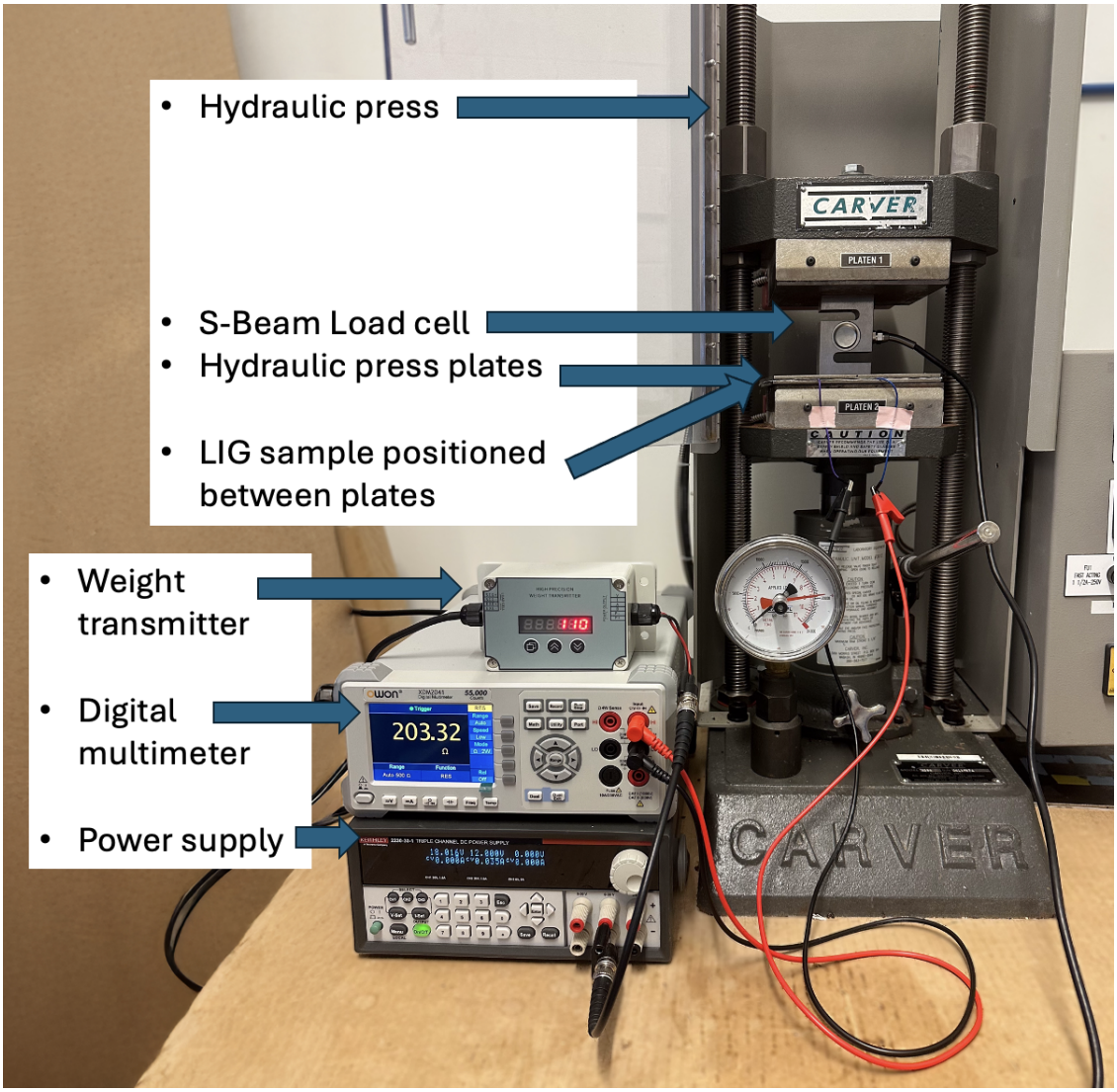

Figure 2.4: The laser process and the resulting LIG structure

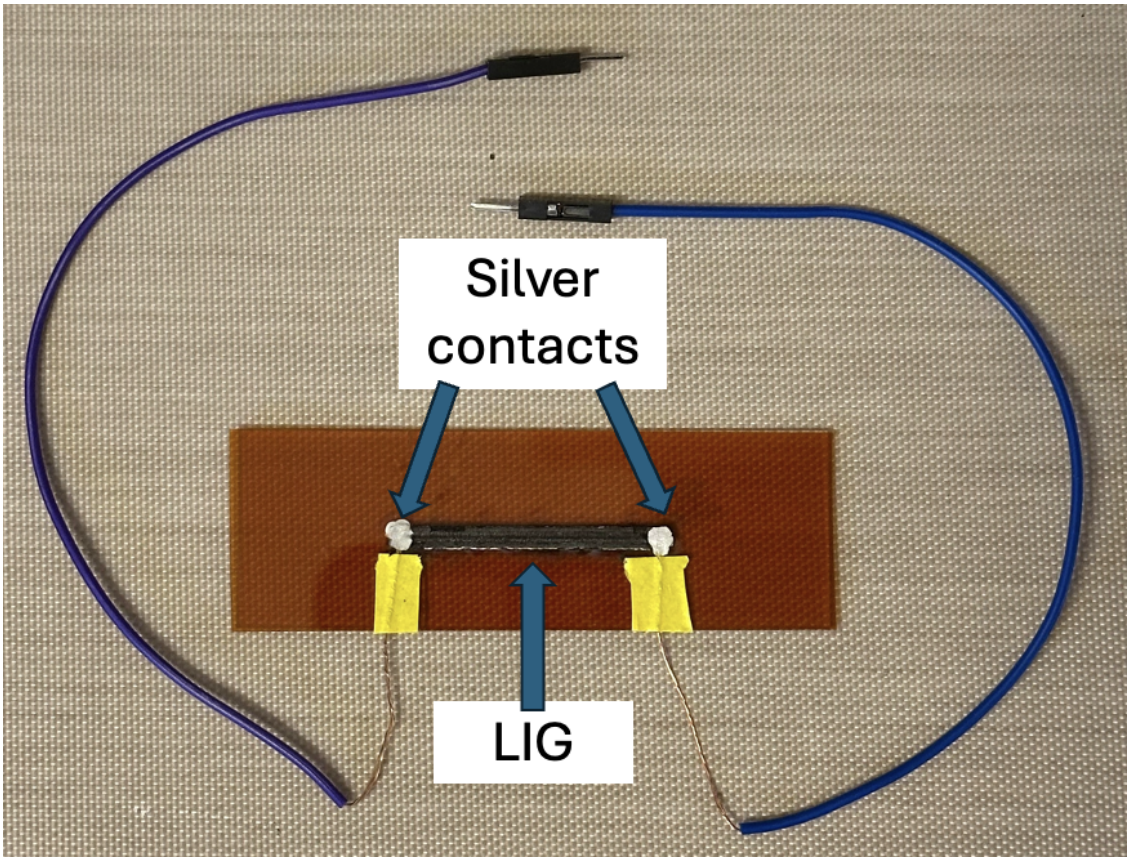

Figure 2.5: The laser process and the resulting LIG structure

the upper plate of the pressing machine which is placed on the sample. This load cell provides instantaneous feedback on the force applied by the hydraulic press, allowing for precise correlation between the applied pressure and the observed changes in electrical resistance. The load cell's readings are synchronized with the resistance measurements from the digital multimeter, enabling a comprehensive analysis of how varying levels of pressure affect the LIG's resistance. This arrangement allows for the controlled application of pressure while simultaneously measuring both the applied force and the resulting changes in electrical resistance.

By integrating these components, our custom-designed system offers several advantages. It allows for real-time data collection, providing insights into the dynamic behavior of LIG under applied force. The inclusion of the load cell ensures accurate quantification of the applied pressure, enabling detailed analysis of the pressure-resistance relationship. The use of silver paint contacts minimizes additional resistance, ensuring that the measured changes are primarily due to the LIG's response to applied pressure. Furthermore, the system's versatility allows it to accommodate various sample sizes and configurations, enabling comprehensive testing of different LIG patterns and encapsulation methods.

This in-situ resistance measurement system represents a significant advancement in the characterization of LIG properties under mechanical stress. By providing real-time, accurate data on the relationship between applied pressure and electrical resistance, it enables a deeper understanding of the encapsulation process and its effects on LIG's electrical properties. The insights gained from this system are crucial for optimizing the encapsulation technique and developing LIG-based devices with enhanced mechanical robustness while maintaining desirable electrical characteristics.

2.4 Four-Point Probe Measurements

To accurately measure the electrical resistance of LIG and eliminate potential contact resistance effects, we implemented the four-point probe technique. This method is crucial for obtaining precise resistance measurements by effectively eliminating the possibility of the influence of contact resistance. Our approach involved a comparative study between the two-point measurement and the four-point probe technique, allowing us to validate the accuracy of our resistance measurements and assess the impact of silver paint contacts on the overall resistance readings. In this experiment, we modified our in-situ resistance measurement setup to accommodate four-point probe measurements. We prepared LIG samples with four silver paint contacts evenly spaced along the length of the LIG structure. The experimental procedure involved conducting resistance measurements under varying applied pressures using both the two-point and four-point methods on the same LIG sample.

We used the high-precision digital multimeter (OWON XDM2041), which offers the capability to switch between two-point and four-point measurement modes. This feature was instrumental in our investigation, allowing us to perform both types of measurements with the same instrument, thereby minimizing potential variability from using different equipment.

To switch the OWON XDM2041 from two-point to four-point measurement mode, we followed a specific procedure. We first ensured that the multimeter was in resistance measurement mode. We then switched from the two-wire (two-point) setting to the four-wire (four-point) setting. Once in four-point mode, the multimeter uses separate pairs of terminals for current supply and voltage measurement. The outer two probes supply the current, while the inner two probes measure the voltage drop across the sample. This configuration allows for the elimination of contact resistance

from the measurement.

During the experiment, we carefully recorded resistance values obtained from both the two-point and four-point measurements at various levels of applied pressure. By comparing these values, we could determine if there was a significant difference between the two methods. If the resistance values were comparable, it would indicate that the contact resistance introduced by the silver paint was negligible under various pressure conditions. Conversely, a noticeable discrepancy would suggest that contact resistance was influencing our measurements, necessitating the use of the four-point probe technique for more accurate results.

This four-point configuration eliminates contact resistance effects due to the fundamental principles of voltage measurement. The key lies in the high input impedance of voltmeters, which means they draw negligibly small currents during measurement. While significant voltage drops occur at the contact points of the current-carrying outer probes due to contact resistance, the voltage-sensing inner probes draw such minimal current that the voltage drops at their contact points are effectively zero. Therefore, the voltage measured between the inner probes reflects only the voltage drop across the sample itself. Since resistance is calculated using this measured voltage and the known current supplied through the outer probes (R = V/I), the result represents the true resistance of the sample, unaffected by contact resistances at any of the probe points. This would not be possible in a two-point measurement, where the same probes carry current and measure voltage, making it impossible to separate the contact resistance from the sample resistance.

Notably, as shown in fig. 3.4, our analysis revealed no significant discrepancy between the two-point and four-point measurements across the range of applied pressures. This consistency

in results strongly suggests that the contact resistance introduced by the silver paint contacts was indeed negligible in our experimental setup. Consequently, we could confidently proceed with our two-point measurement approach for the remainder of our studies, assured that our resistance measurements accurately reflected the intrinsic properties of the LIG samples.

2.5 Raman Spectroscopy

Raman spectroscopy was employed as a powerful tool to investigate the structural characteristics of LIG samples before and after the application of mechanical pressure during encapsulation. This non-destructive technique provides valuable insights into the structure and composition of materials, making it particularly useful for examining potential changes in the graphene structure induced by our encapsulation process.

Our test included the analysis of three LIG samples, each representing a different stage in our study:

- **As-fabricated LIG**: This sample represented the baseline condition, allowing us to characterize the initial structural properties of the LIG immediately after its fabrication.
- **LIG subjected to 80 psi of pressure**: This sample was subjected to a moderate level of pressure, simulating the conditions of our encapsulation process.
- **LIG subjected to 800 psi of pressure**: This sample was exposed to a high level of pressure, enabling us to examine the effects of more extreme mechanical stress on the LIG structure.

It is important to note that for samples 2 and 3, we employed a modified approach to simulate the pressure conditions of encapsulation without actually encapsulating the samples. This methodological adaptation was necessary due to the nature of the Kapton film used in our encapsulation process. The adhesive properties of the Kapton film would have made it impossible to separate the film from the LIG after encapsulation without destroying the LIG structure, thereby making Raman analysis unfeasible.

To overcome this challenge, we devised an alternative method that simulated the pressure conditions while maintaining sample integrity for Raman analysis. We placed a layer of glass on top of the LIG samples before applying pressure. This glass layer acted as a non-adhesive substitute for the Kapton film, allowing us to apply the desired pressure without compromising the ability to perform subsequent Raman spectroscopy. This approach ensured that the LIG samples experienced mechanical stress comparable to the actual encapsulation process while remaining accessible for Raman analysis. Although the glass-top method closely simulates the structural effects of encapsulation, accurately measuring the similarity in electrical resistance between the glass-topped and encapsulated LIG samples is challenging. Specifically, resistance measurements become unreliable once the glass is removed because it immediately changes the resistance of the sample. Therefore, while we cannot provide precise numerical data on resistance comparisons, this method is still the closest to replicating the encapsulation process in terms of applying consistent pressure without altering the structure further. This logical comparison supports the idea that both conditions should have similar structural behaviors, even though direct measurements after pressure application aren't possible.

Raman spectroscopy on these samples provides a lot of information about the graphene structure and its response to mechanical stress. By analyzing the Raman spectra of samples 1, 2, and 3, we can detect several key aspects:

- **Graphene Quality**: The intensity and shape of the G and 2D peaks in the Raman spectra offer insights into the quality and layer structure of the graphene. Changes in these peaks across the samples can indicate alterations in the graphene structure due to applied pressure [51, 52].

- **Defect Density**: The presence and intensity of the D peak in the Raman spectra provide information about defects in the graphene structure. Comparing the D peak across samples can reveal whether mechanical stress induces or alters defects in the LIG [53, 54].

- **Strain Effects**: Shifts in peak positions, particularly of the G and 2D peaks, can indicate strain in the graphene lattice. By comparing these shifts across samples 1, 2, and 3, we can assess how different levels of applied pressure affect the strain state of the LIG [55, 56].

- **Structural Integrity**: The overall shape and relative intensities of the Raman peaks across the three samples can provide information about the structural integrity of the LIG under different pressure conditions. This analysis helps in understanding how well the LIG structure withstands mechanical stress [57, 58].

- **Chemical Changes**: Any new peaks or significant alterations in the Raman spectra of samples 2 and 3 compared to sample 1 could indicate chemical changes induced by the applied pressure, offering insights into potential pressure-induced reactions or transformations in the LIG structure [59, 60].

The Raman spectroscopy measurements were performed using a Bruker SENTERRA Dispersive Raman Microscope operating at a wavelength of 532 nm with a laser power of 5 mW. The microscope was equipped with an objective lens having a numerical aperture (NA) of 0.75, and the measurements were conducted using an aperture of 50×1000 micrometers with a spectral resolution of 9-15 cm^{-1}. By conducting this comprehensive Raman spectroscopy analysis, we aim to gain a deeper understanding of how mechanical pressure, simulating our encapsulation process, affects the structural and chemical properties of LIG. This information is crucial for optimizing our encapsulation technique and for predicting the performance and durability of LIG in various applications where it may be subjected to mechanical stress.

2.6 Scanning Electron Microscopy (SEM)

Scanning Electron Microscopy (SEM) was employed as a crucial analytical technique to observe and characterize the microstructural changes in LIG under varying mechanical loads. This high-resolution imaging method allows for the detailed examination of surface topography and morphology, providing invaluable insights into the structural evolution of LIG in response to applied pressure. Our SEM analysis focused on the same set of samples used in our Raman spectroscopy studies: as-fabricated LIG, LIG subjected to moderate pressure (equivalent to 80 psi pressure), and LIG under high pressure (equivalent to 800 psi pressure). This consistent sample set allows for direct correlation between spectroscopic data and microstructural observations, enhancing the comprehensiveness of our study.

SEM imaging of these samples offers a lot of information about the LIG structure and its

response to mechanical stress. For the as-fabricated LIG, SEM provides a baseline view of the initial porous network structure characteristic of LIG. This includes information about pore size distribution, the interconnectivity of graphene flakes, and the overall surface roughness. These initial observations are crucial for understanding the starting morphology of our LIG samples.

Examination of the LIG sample subjected to moderate pressure reveals how the initial porous structure responds to mechanical compression. SEM images of this sample can show potential changes in pore size, alterations in the orientation of graphene flakes, and any early signs of structural deformation or collapse.

The SEM analysis of the LIG sample under high pressure provides insights into the extreme case of mechanical stress. These images can reveal more dramatic structural changes, such as severe compression of the porous network, potential fracturing or folding of graphene layers, and overall densification of the LIG structure. By comparing the SEM images across these three samples, we can observe the progressive changes in LIG microstructure as a function of applied pressure, providing valuable information for optimizing our encapsulation process.

Furthermore, SEM analysis can reveal surface features that might not be apparent through other analytical methods. For instance, it can show the formation of any surface defects, cracks, or delamination that might occur under pressure. These observations are crucial for assessing the mechanical robustness of LIG and predicting its performance in various applications.

The high magnification capabilities of SEM also allow for the examination of individual graphene flakes and their interfaces. This level of detail can provide insights into how the graphene network deforms and rearranges under pressure, which is essential for understanding the mechanisms behind

any observed changes in electrical or thermal properties.

Chapter 3

Electrical Performance and Mechanical Characterization of Laser-Induced Graphene

3.1 Electrical Performance of As-Prepared LIG

Before examining the effects of mechanical forces on the resistance of LIG, it is crucial to establish the baseline electrical properties of the as-prepared LIG. This baseline allows for meaningful comparison with other works and helps to contextualize the data presented in subsequent sections.

In our work, we prepared 24 LIG samples, with their sheet resistance values ranging between 2.00 $\Omega/square$ and 2.44 $\Omega/square$, with an average of 2.22 $\Omega/square$. This exceptionally low resistance demonstrates the high quality and conductivity of our LIG samples even before any

external stress was applied. To illustrate how favorable these results are, we compare them with other studies in the field.

For example, studies have reported sheet resistances of LIG as low as 32 $\Omega/square$ for materials with porous, weblike structures [37]. In another case, square-patterned LIG electrodes achieved resistances as low as 7.86 $\Omega/square$ [30]. Furthermore, a fabrication method converting 3D-printed polyether-imide (PEI) into graphene via laser exposure resulted in extremely low sheet resistances of 0.30 $\Omega/square$ [61], albeit using much thicker LIG films than ours. Other notable works include studies converting positive photoresist (PR) into LIG, yielding sheet resistances of approximately 120 $\Omega/square$ [62]. Additionally, increasing the laser power from 3.3 W to 4.5 W has been shown to continuously decrease LIG sheet resistance, with highly conductive LIG reaching 15.9 $\Omega/square$ at 4.5 W [63]. Studies utilizing CO_2 lasers on polyimide achieved sheet resistances as low as 6.14 $\Omega/square$ by optimizing energy delivery and pulse overlap [24]. Another study developed a scalable method for creating LIG patterns on diverse substrates, obtaining sheet resistances of around 44 $\Omega/square$ using phenolic resin and inexpensive 405 nm semiconductor lasers [64].

Minhas-Khan et al. discussed several studies on polyimide-based LIG, reporting sheet resistance values in the range of 10–50 $\Omega/square$. By optimizing pulse overlap and energy delivery, their work achieved a sheet resistance of 6.14 $\Omega/square$ with a CO_2 laser [65]. Additionally, for biomedical applications, Zhu et al. used electroless plating techniques to coat LIG with various uniform metals, achieving good conductance of 25 $\Omega/square$ for glucose sensing in diabetic patients [66]. It is important to note that variations in the reported sheet resistances of LIG among different studies can be attributed to differences in LIG thickness too. In our experiments, the LIG thickness was more

than 125 µm, assuming complete consumption of the Kapton substrate during the laser processing. This parameter is critical as LIG thickness can influence electrical conductivity [62]. For a fair comparison with other reports, it is essential to consider that the LIG samples in some studies might have different thicknesses, which can affect their electrical properties. Understanding these variations is crucial for assessing the true performance enhancements achieved through different fabrication methods and conditions.

To provide a clear comparison of the sheet resistance achieved in our work with that reported in other studies, we have compiled table 3.1. This visualization helps in highlighting how our fabrication techniques measure up against existing methods in the field of LIG.

It is clear from this comparison that the LIG samples prepared in our study exhibit very high conductivity, with much lower sheet resistance than many comparable works. This provides a strong foundation for further analysis, particularly when assessing how much the resistance is increasedunder pressure.

Our comparative analysis from table 3.1 clearly demonstrates that the LIG samples produced in our study exhibit lowest sheet resistance recorded among all studies utilizing this laser equipment for inducing graphene. This significantly low sheet resistance of our samples provides a robust foundation for further analysis, particularly in assessing how much the resistance increases with pressure. Notably, the closest competing work reported a low sheet resistance of 0.3, achieved through another method involving the conversion of 3D-printed polyether-imide (PEI) into graphene via scanned laser exposure [61].

Additionally, the fragile nature of LIG structures was demonstrated by rubbing the surface of

Table 3.1: Comparison of sheet resistance values from various studies

Sheet Resistance (ohm/square)	**Reference**
2.00 to 2.44	Our Work
32.00	[37]
7.86	[30]
0.30	[61]
130.00	[43]
120.00	[62]
15.90	[63]
6.14	[24]
44.00	[64]
10.00 to 50.00	[65]
25.00	[66]

the as-prepared samples, which resulted in a noticeable increase in sheet resistance. While we acknowledge that rubbing with a fingertip is not a fully quantifiable method—since factors such as the force applied, speed, and pressure of rubbing cannot be consistently measured—this serves as a simple demonstration to highlight the fragile nature of the LIG structure. This sensitivity to mechanical disruptions could negatively impact its electrical performance, reinforcing the importance of encapsulation in some applications. By presenting this baseline, we provide a clearer context for understanding the subsequent results regarding the effects of mechanical forces on LIG resistance, as discussed in the following sections.

Before starting the next section, where we talk about the systematic pressure testing, we conducted a preliminary experiment to demonstrate the fragility of as-made LIG. We measured the sheet resistance of an LIG sample, then rubbed it with a finger, applying a mild pressure, and measured the resistance again. As shown in Table 3.2, even this basic contact caused notable changes in the sheet resistance, up to 130% increase in initial resistance. While this test wasn't very precise - we couldn't control exactly how fast, how hard, or at what angle we rubbed the surface - it clearly showed how sensitive unprotected LIG is to physical contact. Figure 3.1 shows pictures of the LIG surface before and after rubbing, clearly displaying these changes.

3.2 Effect of Applied Force on Resistance

This section presents the results and analysis of our investigation into the resistance changes of LIG under various applied mechanical forces, without encapsulation. Our study aimed to understand the behavior of LIG when subjected to external pressure, providing crucial insights into its electrical properties under mechanical stress. The experimental process began by placing the fabricated LIG sample, with silver paint contacts, under a glass cover to ensure uniform pressure. The assembly was then placed in a hydraulic press equipped with a load cell above to accurately measure the applied pressure.

Our experimental protocol involved manually increasing the applied pressure on different LIG samples with the same speed, covering a wide range of pressure from 80 psi to 3800 psi. This comprehensive range allowed us to observe and analyze the LIG's electrical response across a spectrum of mechanical stresses, from relatively mild to extreme pressures. The in-situ resistance

Table 3.2: Effect of rubbing on electrical resistance of LIG samples. The resistance before column indicates the initial resistance of LIG samples, and resistance after shows the resistance after rubbing with a finger.

Resistance Before (ohm)	**Resistance After (ohm)**	**Percent Increase (%)**
35.6	71.4	101%
41.2	62.5	52%
39.5	88.9	125%
43.2	67.9	57%
38.4	86.1	124%
43.6	82.1	88%
37.6	77.2	105%
40.4	93.1	130%
45.2	68.2	51%
39.5	80.6	104%

Figure 3.1: Effect of finger rubbing on the structure of a laser-induced graphene (LIG) sample. The left image shows the sample before rubbing, and the right image shows the sample after rubbing.

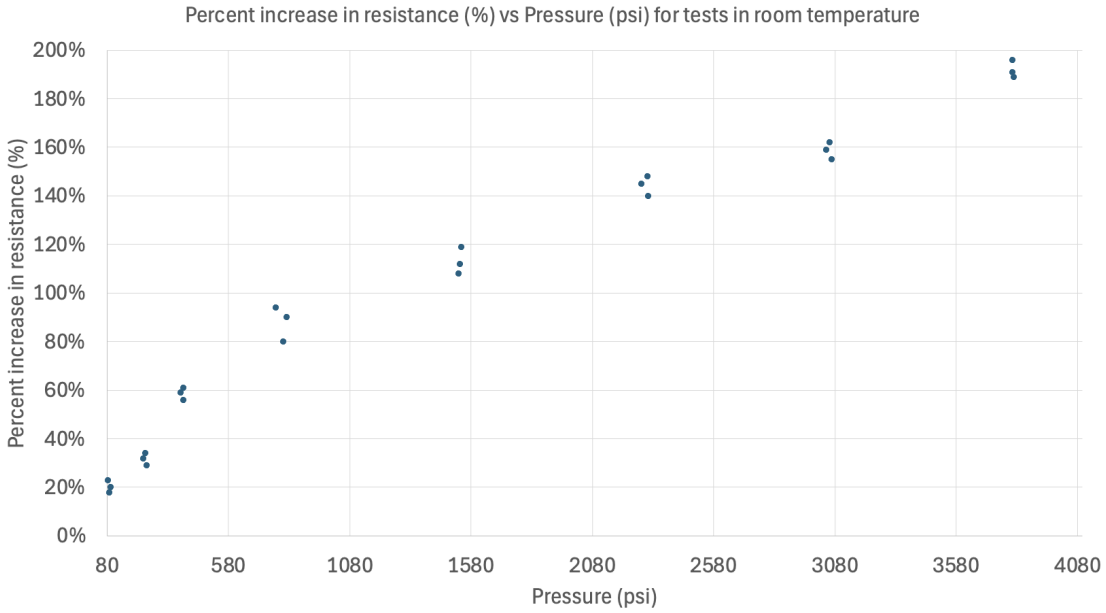

Figure 3.2: The relationship between applied pressure (psi) and the percent increase in total resistance (%) of LIG samples. Each data point represents a different sample.

measurements provided real-time data on how the resistance of LIG changed with increasing pressure.

As shown in Figure 3.2, our results reveal a consistent, non-linear relationship between applied pressure and the percent increase in resistance of LIG samples. At lower pressures around 80 psi, we observed relatively small changes in resistance, with increases ranging from approximately 18% to 23%. This suggests that at these lower pressures, the LIG structure largely maintains its integrity and conductive pathways. As the pressure increases, we see a consistent upward trend in resistance change, indicating gradual structural modifications within the LIG network. The data demonstrates a non-linear trend in resistance changes across the pressure range. At moderate pressures around 1580 psi, the resistance increase falls within the 110% to 120% range. This non-linearity becomes more

obvious at higher pressures, with the 3080 psi mark showing resistance increases between 155% and 162%. The most dramatic changes are observed at the highest tested pressure of about 3800 psi, resulting in resistance increases of 185% to 195%. The higher rate of change in lower pressures suggests a complex mechanism, likely involving the progressive compression of the porous LIG structure and potential changes in the contact between graphene flakes. The consistency of the trend and the relatively small spread of data points at each pressure level indicate good reproducibility and uniform response of the LIG samples to applied pressure.

These findings have significant implications for the practical application of LIG in various fields, particularly in pressure-sensing devices. The non-linear response provides a wide dynamic range for sensing, with higher sensitivity at lower pressures that gradually decreases at higher pressures. This characteristic makes LIG ideal for applications requiring precise detection in low-pressure environments while remaining effective under higher pressures. Additionally, the data contributes to our understanding of the fundamental properties of LIG, highlighting the complex relationship between its porous structure and electrical resistance under compression. This predictable non-linear response also facilitates accurate calibration, enhancing the potential versatility of LIG-based devices in applications subject to varying mechanical stresses.

3.3 Cyclic Loading and Unloading

In this section, we present the findings from our investigation into the behavior of LIG resistance under repeated cycles of loading and unloading mechanical forces. This study provides crucial insights into the material's resilience and the stability of its electrical properties under dynamic

mechanical stress conditions, which is essential for understanding its potential in applications involving repeated mechanical strain. Building upon our experiment of applying pressure to LIG samples in the previous section, we extended our experiment to include multiple cycles of loading and unloading.

As shown in Fig 3.3, our observations reveal a complex pattern of resistance changes across loading cycles, with a distinct first-cycle behavior followed by more consistent subsequent cycles. To aid in understanding these patterns, each graph is annotated with numbered paths (1-5) and directional arrows, where red path 1 represents the initial loading cycle, red path 2 shows the first unloading cycle, and subsequent paths (3-5) show additional loading and unloading cycles in alternating colors. The start and end points are clearly marked to show the progression of resistance changes over time. During the initial loading cycle (path 1, red), we observed a significant irreversible increase in resistance, ranging from approximately 20% at 80 psi to as high as 190% at 3875 psi. This substantial initial change aligns with our findings from the previous section and represents a permanent alteration in the LIG structure. It is important to note that the majority of the resistance increase on the first loading cycle takes place during the unloading phase (path 2, red). Following this initial irreversible change, subsequent loading cycles (paths 3-5) displayed a different pattern. In these later cycles, applying pressure caused the resistance to decrease from the value established after the first unloading. Upon releasing the pressure, the resistance returned to a value close to, but slightly higher than, the resistance after the first loading. This pattern was consistent across all pressure ranges tested, from 80 psi to 3875 psi, with the magnitude of resistance changes varying with applied pressure. The behavior observed in the higher pressure ranges (1600 psi and 3875 psi)

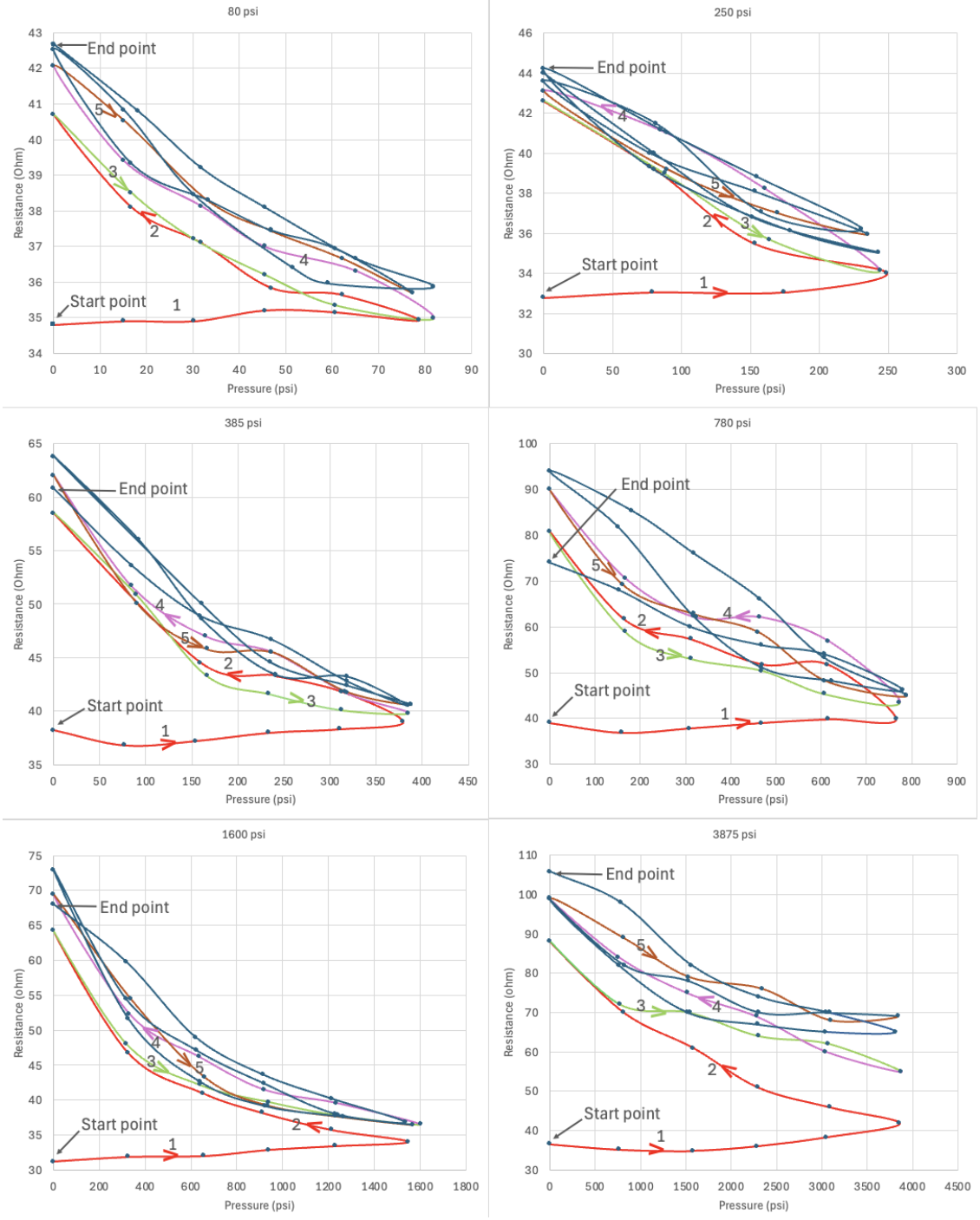

Figure 3.3: Behavior of LIG resistance under repeated cycles of pressure loading and unloading. The different panels represent experiments at varying target pressures.

follows the same general pattern but with more pronounced effects. At these elevated pressures, the initial resistance increase during the first cycle is particularly dramatic, and the subsequent cycles show larger amplitude changes in resistance during loading and unloading. Despite the higher pressures, the cyclic behavior remains relatively consistent after the initial conditioning cycle, though with greater absolute changes in resistance values. These findings have significant implications for the application of LIG in devices or systems that may undergo repeated mechanical stress. The large, irreversible change in the first cycle suggests a fundamental restructuring of the LIG under initial loading. The subsequent cycles, showing reversible decreases in resistance under load and near-complete recovery upon unloading, indicate that the LIG maintains a degree of elasticity after its initial structural change. However, the slight growing increase in resistance over multiple cycles after unloading points to ongoing, though much smaller, structural changes with repeated use. For applications involving cyclic loading, these results highlight the need for a "conditioning" phase to stabilize the LIG's electrical properties. After this initial conditioning, the material demonstrates relatively stable and predictable behavior, which is promising for long-term use in flexible or pressure-sensitive devices. However, designs requiring precise and stable electrical properties should account for both the initial large change and the smaller, ongoing shifts in baseline resistance over extended use.

3.4 Role of Contact Resistance

The results of our comparative study between two-point and four-point probe measurements are presented in Figure 3.4. This graph illustrates the percent change in resistance for LIG samples

under various applied pressures, comparing data obtained from both measurement techniques.

Our analysis reveals a strong correlation between the two-point (circles) and four-point (squares) measurements across the entire pressure range. This consistency validates the assumption that the contact resistance introduced by the silver paint contacts is negligible in our experimental setup. Both measurement techniques show a non-linear increase in resistance as pressure increases, with the percent change in resistance rising from approximately 20% at low pressures to nearly 200% at the highest pressure tested. The close alignment of two-point and four-point measurements, each representing an average of three data points, demonstrates excellent reproducibility in our experimental results. This reproducibility enhances the reliability of our findings and the robustness of our measurement techniques.

While the overall trend is consistent, we observe minor differences between the two-point and four-point measurements at certain pressure points. These small discrepancies could be attributed to inherent material variability or minor experimental uncertainties, rather than systematic differences between the measurement techniques. The close agreement between two-point and four-point measurements across the entire pressure range validates our use of the simpler two-point method for subsequent experiments. This confirmation is particularly valuable as it allows for more straightforward experimental setups in future studies without compromising measurement accuracy.

3.5 Effect of Temperature on Resistance

To investigate the influence of temperature on the resistance of LIG when pressure is applied, we repeated the same experiment as in Section 3.2, this time utilizing the temperature control

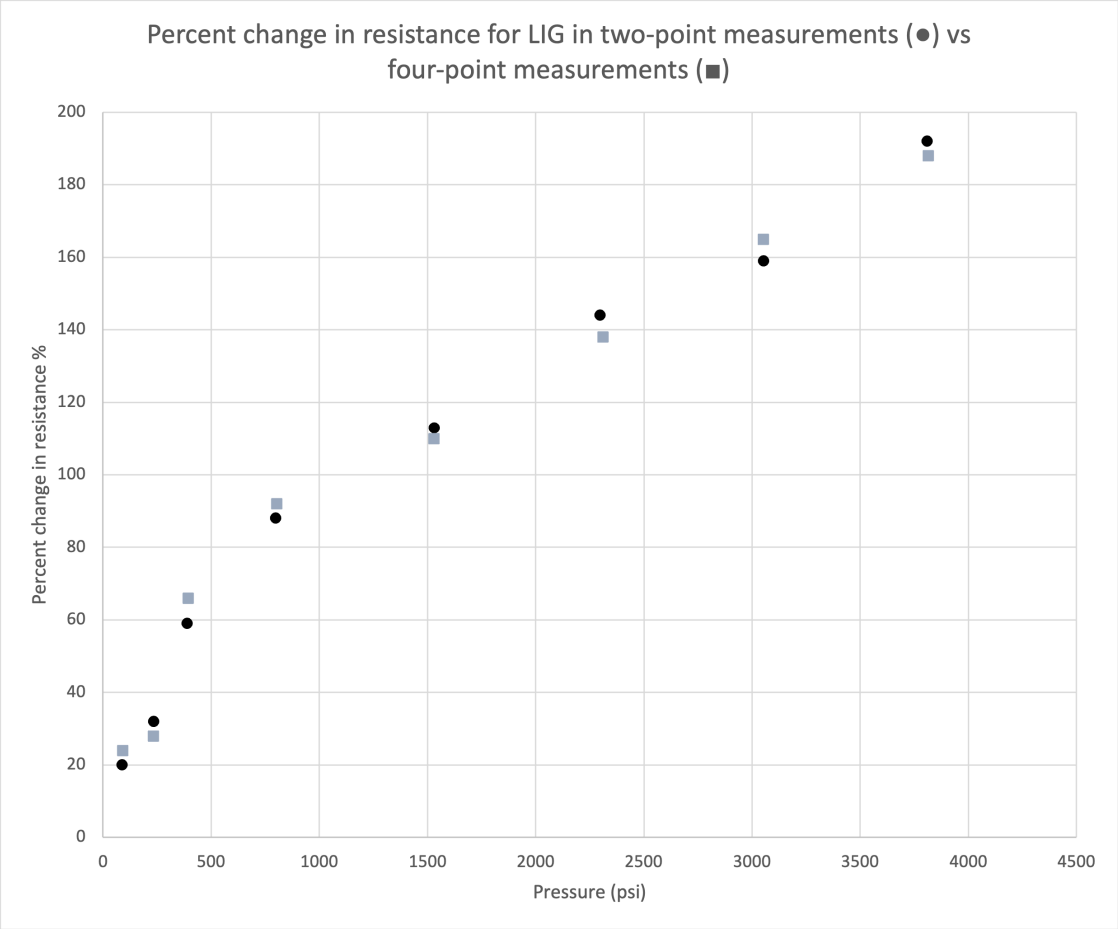

Figure 3.4: Percent change in resistance of LIG under varying pressure, comparing two-point (●) and four-point (■) measurement techniques to eliminate the possibility of contact resistance effect in the measurements. Each point represents an average of three measurements.

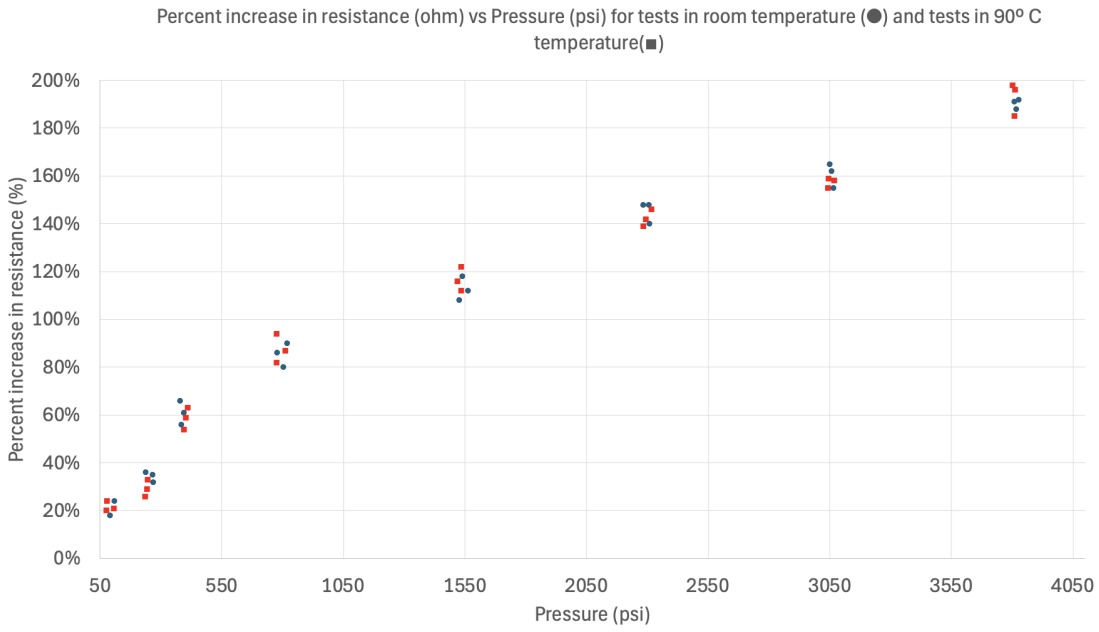

Figure 3.5: Percent change in resistance of LIG under varying pressure, in room temperature (●) and elevated 90° C temperature (■) to investigate the effect of temperature on the measurement results.

capabilities of the hydraulic press. We set the temperature to 90 degrees Celsius, a limit chosen to prevent damage to the Kapton substrate and wire contacts, which are susceptible to degradation at higher temperatures. Each LIG sample was allowed to equilibrate at this elevated temperature for 10 minutes before testing, ensuring uniform heating throughout the material. Following the temperature equilibration, we applied the same pressure application procedure used in our previous room temperature tests in Section 3.2. Resistance measurements were recorded in real-time as we gradually increased the applied pressure on the LIG samples. This approach allowed for a direct comparison between the high-temperature data and our earlier room temperature results.

The three points showing the LIG samples at room temperature are the exact same points in Section 3.2. Interestingly, our observations revealed that the increase in temperature to 90 degrees

Celsius did not significantly alter the resistance of LIG under applied pressure. The resistance changes observed at this elevated temperature closely mirrored those seen in our room temperature tests. This consistency across temperature conditions suggests that LIG maintains its electrical properties and response to mechanical pressure even at moderately elevated temperatures.

3.6 Durability Against Moisture

To evaluate the moisture resistance of encapsulated LIG, we immersed samples encapsulated at 80 psi in water for 24 hours to simulate long-term exposure to wet conditions. The observed increase in electrical resistance was minimal, at only 1.7%, demonstrating that our encapsulation method substantially preserves the conductivity of LIG against moisture. This result highlights the potential of encapsulated LIG for applications in outdoor or harsh environmental conditions, as shown in table 3.3.

To establish a baseline for comparison, identical moisture tests were performed on non-encapsulated LIG samples, which exhibited a higher resistance increase of up to 3.7%. The results for these non-encapsulated LIG samples are detailed in table 3.4. This comparison underscores the effectiveness of our encapsulation technique in enhancing the moisture resistance of LIG, confirming its suitability for use in environments where exposure to moisture is a concern, despite the initial minimal changes in resistance."

This revision incorporates specific references to the charts where the data can be visually reviewed, which helps in providing a clear, structured presentation of your findings in the thesis.

These findings have important implications for the practical application of LIG in various settings.

Table 3.3: Durability Against Moisture – Encapsulated LIG

Resistance before immersion (ohm)	**Resistance after immersion (ohm)**	**% increase**
42.1	42.6	1.2%
39.5	39.6	0.3%
40.2	40.9	1.7%
41.4	42.0	1.4%
46.8	47.0	0.4%
38.6	38.9	0.7%
45.6	46.1	1.1%
43.6	44.3	1.6%
45.4	45.9	1.1%
39.7	39.9	0.5%

Table 3.4: Durability Against Moisture – Non-Encapsulated LIG

Resistance before immersion (ohm)	**Resistance after immersion (ohm)**	**% increase**
38.9	39.6	1.8%
34.5	34.7	0.5%
42.4	43.2	1.8%
40.9	41.8	2.2%
35.0	36.3	3.7%

The stability of LIG's electrical properties at elevated temperatures indicates its potential suitability for applications in environments with fluctuating temperatures. However, it's important to note that our study was limited to 90 degrees Celsius due to material limitations. Further research into LIG's behavior at more extreme temperatures, possibly using different substrate materials, could provide additional insights into its thermal-electrical properties and expand its potential application range.

To date, in-situ measurements of resistance versus pressure for laser-induced graphene have not been reported in the literature. This gap underscores the novelty of our approach, providing a unique contribution to the field of graphene research as detailed in the upcoming sections.

Chapter 4

Encapsulation and Mechanical Robustness

4.1 Encapsulation Method

The encapsulation of LIG with a Kapton layer was developed to enhance its mechanical robustness. This process involved applying a single layer of sticky Kapton tape, 125 micrometers thick, directly onto the fabricated LIG structure. The adhesive side of the tape was carefully placed on the LIG, ensuring smooth application without exerting additional pressure on the delicate graphene structure. To complete the encapsulation, the LIG sample with the applied Kapton layer was subjected to a hydraulic press. This step mirrored the process described in Chapter 3.2, where various pressure levels were applied to different samples. The controlled pressure application served to securely bond the Kapton layer to the LIG, effectively encapsulating the structure. The journey to this successful method involved several unsuccessful attempts, which provided valuable insights. Initially, non-sticky Kapton was tested, with the hypothesis that pressure alone would be sufficient

for encapsulation. However, even under high pressures of up to 3800 psi, the non-sticky Kapton failed to adhere properly and could be easily removed with minimal contact.

Further experiments explored the combination of pressure and heat, with the idea being that heat would cause the Kapton to soften and more conformally adapt to the substrate topography. A temperature of 90 degrees Celsius was applied alongside 3800 psi of pressure, adhering to the thermal limitations outlined in section 3.5. Despite these efforts, the non-sticky Kapton still failed to bond effectively with the LIG structure. It's worth noting that Kapton has a higher glass transition temperature, so 90°C was likely insufficient to induce the desired softening effect. A different polymer with a lower glass transition temperature might be more successful with this approach. Although attempts were made at higher temperatures, they were ultimately constrained by the thermal limitations of the overall system.

These failed attempts highlighted the crucial role of adhesion in the encapsulation process. The ease with which the non-sticky Kapton detached, even under extreme pressure and moderate heat, demonstrated that mechanical force and temperature alone were insufficient for creating a robust encapsulation. The lessons learned from these experiments led to the adoption of sticky Kapton tape as the optimal solution. This approach combined the inherent adhesive properties of the tape with the applied pressure, resulting in a secure and durable encapsulation of the LIG structure. The success of this method underscores the importance of adhesion in achieving effective encapsulation and enhancing the mechanical robustness of LIG.

Notably, the results demonstrated that using sticky Kapton tape enabled highly efficient encapsulation even at relatively low pressures. Samples subjected to as little as 80 psi of pressure

exhibited remarkable adhesion and durability. The success at lower pressures not only simplifies the encapsulation process but also minimizes the risk of damaging the delicate LIG during fabrication.

4.2 Resistance Measurements after Encapsulation

Following the encapsulation process detailed in section 4.1, the resistance of the LIG samples was measured under various mechanical loads. This experiment aimed to assess the impact of encapsulation using different pressures on the electrical properties of LIG.

The experimental procedure closely mirrored that described in section 3.2, where samples were subjected to a range of pressures using a hydraulic press. However, in this case, the LIG samples were first encapsulated with a Kapton layer as per the method outlined in section 4.1. This step allowed for a comparative analysis between the bare and encapsulated LIG structures.

Resistance measurements were taken at each pressure point, providing insights into how the encapsulation layer affected the LIG's electrical performance under a range of pressures. The data collected offered a comprehensive view of the relationship between applied pressure and resistance in the encapsulated samples, allowing for direct comparison with the results obtained from non-encapsulated LIG. These measurements served a dual purpose: firstly, to determine whether the encapsulation process itself had any significant impact on the resistance of the LIG, and secondly, to assess how the encapsulated structure responded to varying degrees of mechanical load. The results of this investigation provide crucial information for understanding the practical applications and limitations of encapsulated LIG in scenarios where both electrical conductivity and mechanical robustness are essential.

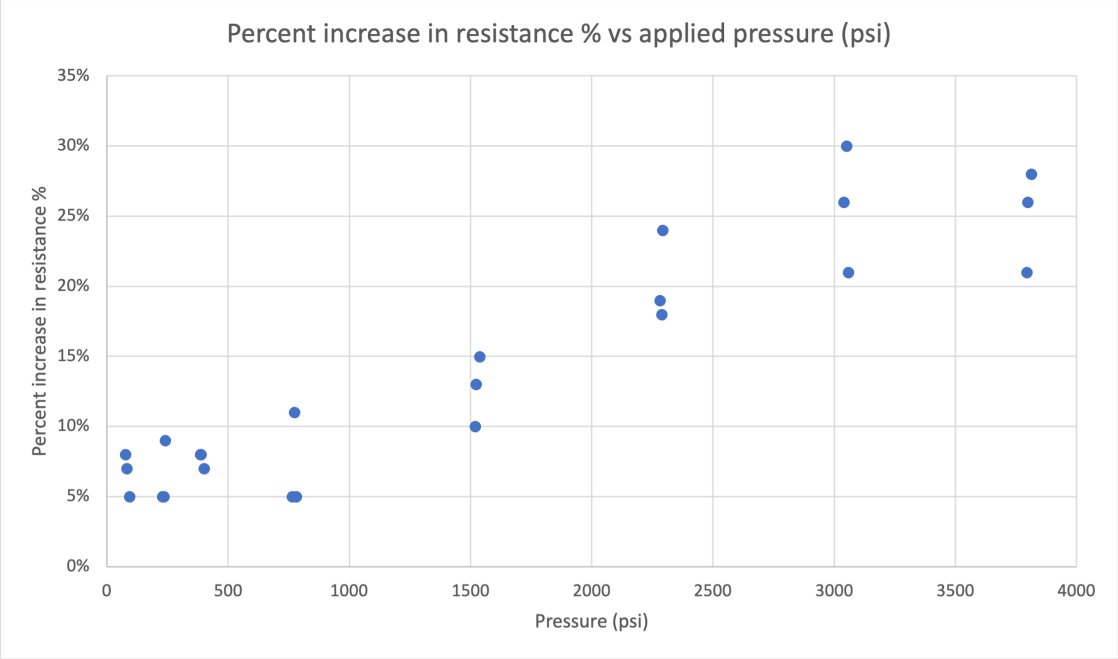

Figure 4.1: Percent increase in resistance of encapsulated LIG samples as a function of applied pressure.

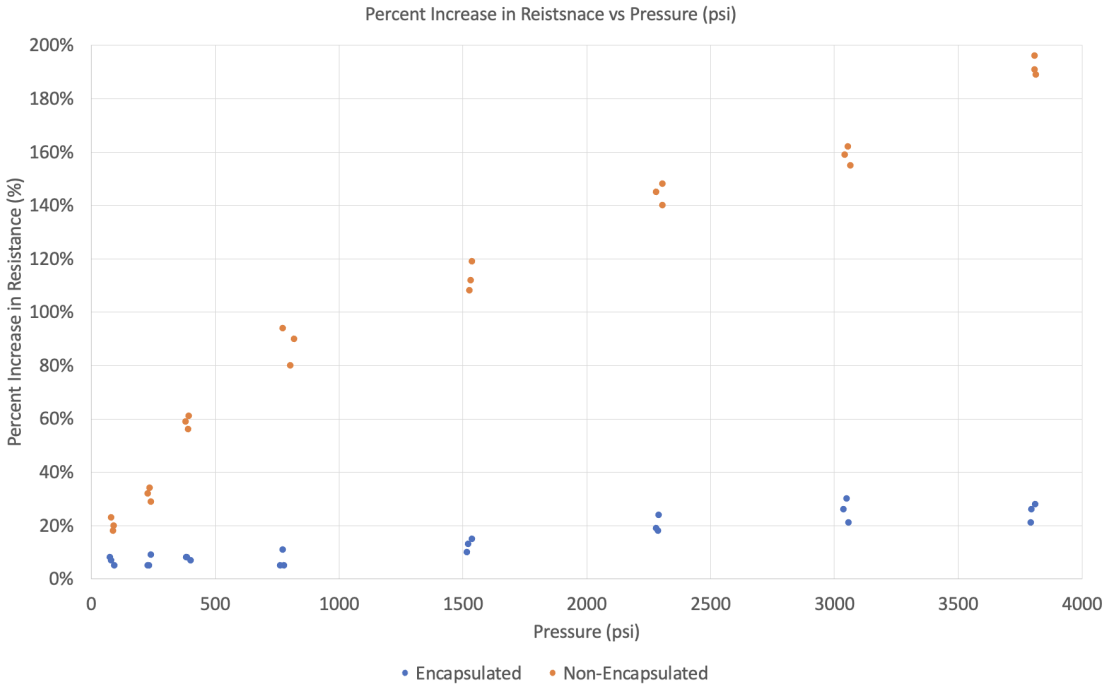

Figure 4.2: Percent increase in resistance of encapsulated LIG samples as a function of applied pressure. The data is compared to LIG without encapsulation, demonstrating improved stability compared to non-encapsulated samples.

The results shown in Fig. 4.1 reveal a significant improvement in the stability of electrical properties compared to non-encapsulated samples. As shown in Figure 4.1, the percent increase in resistance for encapsulated LIG ranges from approximately 5% to 30% across the tested pressure range of 0 to 4000 psi. This range is substantially lower than the 20% to 190% increase observed in non-encapsulated samples, as presented in Fig. 3.2. At lower pressures (below 1000 psi), the encapsulated samples show a modest increase in resistance, generally between 5% and 10%. As the pressure increases, we observe a gradual rise in the resistance change, with most data points falling between 10% and 20% for pressures up to 2500 psi. The highest resistance changes, ranging from 20% to 30%, are observed at the upper end of the pressure spectrum, between 3000 and 4000 psi. This behavior indicates that the Kapton encapsulation layer effectively reduces the pressure-induced changes in LIG's electrical properties. The encapsulation appears to provide a protective barrier that limits the structural deformation of the LIG under pressure, resulting in more stable resistance values across a wide pressure range. This enhanced stability is particularly evident when compared to the non-encapsulated samples, as presented in Fig. 4.2, which exhibited much larger and more rapid increases in resistance under similar pressure conditions. The protective effect of Kapton encapsulation likely stems from its material properties. Kapton's elasticity, in contrast to rigid materials like glass, plays a crucial role. This property allows for better force distribution, preventing localized stress points that could damage the LIG. The Kapton layer absorbs and spreads pressure while confining the LIG structure.

The data also suggests a non-linear relationship between applied pressure and resistance change in encapsulated samples, which is like the relationship between applied pressure and resistance change

in unencapsulated samples as presented in section 3.2. This non-linearity could be attributed to the complex manner in which structural changes modify the interconnected nature of the conductive network. As the network undergoes deformation and disruption due to applied pressure, the resistance correspondingly changes. This explanation accounts for the observed non-linear response in both encapsulated and unencapsulated samples, highlighting the fundamental behavior of the LIG's conductive structure under pressure, regardless of the presence of an encapsulation layer. The reduced sensitivity to pressure changes in encapsulated LIG suggests that encapsulated LIG may be more suitable for applications requiring stable electrical properties under varying mechanical pressures. This characteristic makes encapsulated LIG potentially more appropriate for applications prioritizing stability and durability over high pressure sensitivity.

In the context of previous studies, the sheet resistance of bare graphene (BG) was observed to increase from 1.5 $k\Omega$/sq to 15.9 $k\Omega$/sq when encapsulated with thermal evaporation (TE) SiO2, and from 3.1 $k\Omega$/sq to 341.4 $k\Omega$/sq with pulsed electron deposition (PED) SiO2 encapsulation, highlighting the substantial impact of encapsulation methods on electrical properties. [67] Similarly, an analysis of Laser LIG composites shows that laminating LIG with various materials using a commercial Amazon thermal laminator significantly affects their resistance. In this study, the resistance increased from 0.13 $k\Omega$/sq to 0.44 $k\Omega$/sq for LDPE/LIG/LDPE, to 0.47 $k\Omega$/sq for both LDPE/LIG/HDPE and Duct Tape/LIG/LDPE, to 0.57 $k\Omega$/sq for LDPE/LIG/Cheesecloth, to 0.68 $k\Omega$/sq for LDPE/LIG/Kimwipe, and to 0.76 $k\Omega$/sq for LDPE/LIG Pattern/LDPE, demonstrating at least a 238% increase in resistance for the LDPE/LIG/LDPE composite. [43]

The data in Fig. 4.2 offers a direct visual comparison of the resistance changes in both

encapsulated and non-encapsulated LIG samples under pressure. In this figure, circle markers represent the encapsulated samples, while square markers show the non-encapsulated samples with significantly higher change in resistance. The non-encapsulated samples are shielded by a glass layer that simply rests on the sample surface, providing minimal structural protection without encapsulating it. This chart highlights the difference in resistance change between encapsulated and non-encapsulated samples.

This study is the first to achieve encapsulated laser-induced graphene starting from an initial resistance as low as 2 ohms per square and maintaining minimal resistance increase post-encapsulation. Such low resistance levels enhance its practicality, allowing for its integration into circuits where durability is critical. The subsequent sections will detail how these properties facilitate LIG's use in harsh environments such as water immersion and mechanical stress, without compromising its electrical integrity.

In conclusion, the encapsulation process has demonstrably enhanced the mechanical robustness of LIG while maintaining its conductive properties. This improvement in stability under pressure opens up new possibilities for LIG in applications where consistent electrical performance under mechanical stress is crucial, such as in flexible electronics or wearable devices subject to frequent bending or compression.

4.3 Mechanical Bending Tests

Our previous findings revealed that encapsulated LIG exhibited a resistance increase of only 5 to 30 percent under varying pressures, significantly lower than non-encapsulated samples. While these

results suggest that lower encapsulation pressures are preferable for maintaining electrical properties, they raise questions about the mechanical robustness of the resulting structure. To address this crucial balance between electrical performance and mechanical durability, we designed a bending test. This investigation involved subjecting LIG samples encapsulated at different pressures to bending stress over three cylinders of varying diameters. Our aim was to identify the encapsulation pressure that provides the optimal combination of electrical stability and mechanical flexibility, essential for practical applications like flexible electronics and wearable devices.

To conduct these tests, we prepared LIG samples encapsulated at various pressures within the 80 psi to 3800 psi range. The experimental setup involved three cylindrical objects with diameters of 15, 30, and 45 mm, chosen to represent a range of bending radii. These cylinders served as forms around which the encapsulated LIG samples were bent, allowing for a systematic assessment of their performance under various degrees of curvature.

The testing procedure involved bending each LIG sample over one specific cylinder diameter. Different samples were used for each diameter (15, 30, and 45 mm) to ensure that previous bending didn't influence the results, as bending was found to affect the samples' resistance. During each bending event, the electrical resistance was measured in-situ to find the resistance before and after bending, allowing us to calculate the percentage change in resistance. This approach provided crucial data on how different bending radii affected the electrical properties of samples encapsulated at various pressures. By focusing on the percent change in resistance, we could directly compare the performance of samples across different encapsulation pressures and bending radii, providing insights into the optimal encapsulation conditions for maintaining electrical stability and mechanical

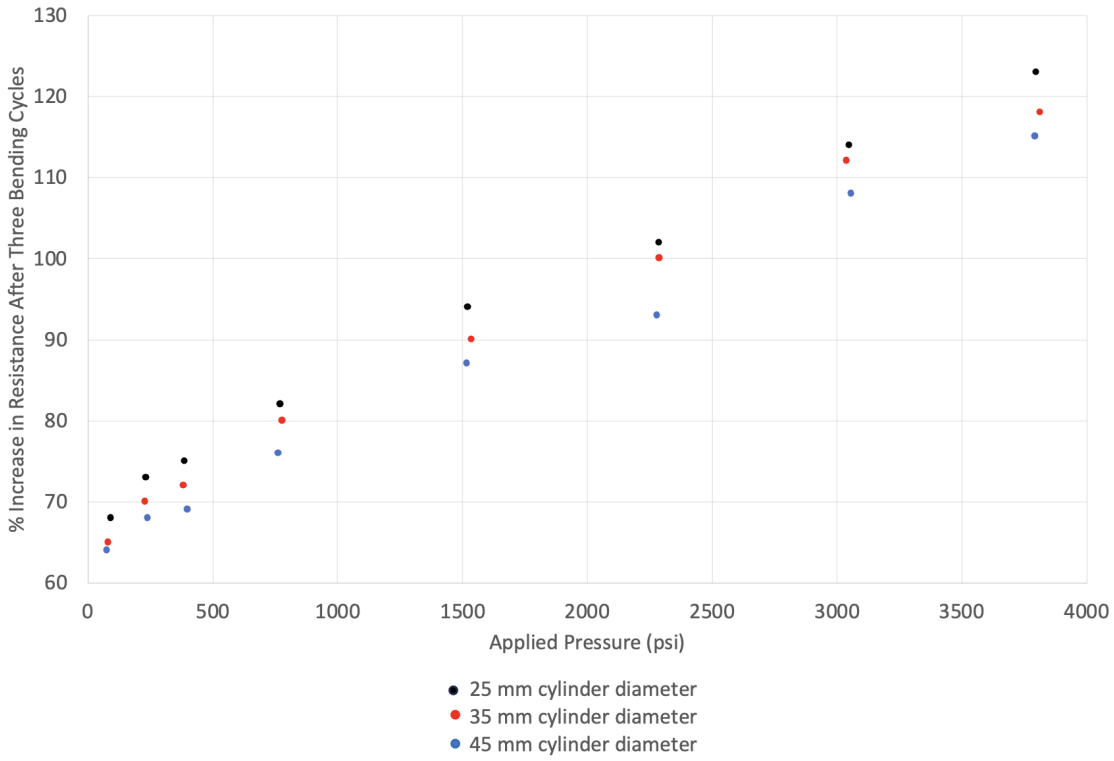

Figure 4.3: Correlation between applied encapsulation pressure and percentage increase in resistance, measured upon completion of three full bending cycles.

robustness. To ensure reliability and assess the repeatability of the results, each bending test was performed three times for every cylinder diameter and encapsulation pressure. This repetition served to identify any potential degradation or fatigue in the samples over multiple bending cycles, while also revealing how different encapsulation pressures affected the LIG's flexibility and electrical stability.

The results presented in Table 4.1 and Fig. 4.3 reveal a clear trend in the relationship between applied encapsulation pressure and the electrical stability of LIG samples under bending stress. As the encapsulation pressure increases from 80 psi to 3798 psi, there's a consistent rise in the

Table 4.1: Effect of encapsulation pressure on electrical resistance of LIG samples after bending. The applied pressure column indicates the pressure used during encapsulation. Columns 1B, R, 2B, R, 3B, R indicate the resistance during first, second and third bends interleaved with the resistance after each bend was released, in units of Ohms.

Applied Pressure (psi)	**Resistance After Encapsulation (Ohm)**	**Bend Diameter**	**1B**	**R**	**2B**	**R**	**3B**	**R**	**Percent Increase in R After 3 Times Bending**	**Average**
93	40	25mm	41	65	41	66	42	67	68%	66%
80	45	35mm	44	67	45	68	46	70	65%	66%
77	42	45mm	41	66	42	68	42.5	69	64%	66%
234	42	25mm	40	71	41	72	42	73	73%	70%
229	40	35mm	39	66	40	66	40.5	68	70%	70%
241	48	45mm	48	80	49	80	50	81	68%	70%
388	42	25mm	41	73	42	73	43	74	75%	72%
385	40	35mm	41	66	42	68	42.5	69	72%	72%
401	45	45mm	46	74	47	75	47	76	69%	72%
773	40	25mm	42	69	43	71	45	73	82%	79%
780	43	35mm	43	75	44.5	76	45	77	80%	79%
764	42	45mm	43	71	44	73	45.5	74	76%	79%
1523	44	25mm	45	83	45.5	84	45	85	94%	90%
1538	46	35mm	47	85	47.5	85	47	87	90%	90%
1518	46	45mm	45	85	46	86	46	86	87%	90%
2289	46	25mm	44	90	45	91	47	93	102%	98%
2292	47	35mm	46	90	46	92	48	94	100%	98%
2281	50	45mm	52	96	51	96	52	97	93%	98%
3050	52	25mm	50	108	52	110	51	111	114%	111%
3039	49	35mm	50	101	51	102	53	104	112%	111%
3058	51	45mm	50	105	52	105	54	106	108%	111%
3798	53	25mm	52	115	53	116	51	118	123%	119%
3813	50	35mm	51	103	52	105	54	106	118%	119%
3795	52	45mm	54	109	55	111	57	112	115%	119%

percentage increase of resistance after bending from 64% to 123%. Moreover, as the bend diameter increases, the changes in resistance generally lowered. This suggests that less severe bending (larger diameter) causes less disruption to the electrical properties of the encapsulated LIG samples.

Fig. 4.3 visually reinforces this trend, showing a clear positive correlation between applied pressure and the percentage increase in resistance after bending. The data points show an overall upward trend on the y-axis as the applied pressure increases along the x-axis, with some scatter at each pressure level. This pattern suggests that higher encapsulation pressures generally lead to greater increases in electrical resistance when the material is subjected to bending stress, though there is variability in the response at each pressure point.

Based on these results, the optimal pressure for encapsulation appears to be in the lower range, between 80-400 psi. This range offers a balanced compromise between mechanical protection and electrical stability. Samples encapsulated at these pressures show a relatively modest increase in resistance (around 64-75%) after 3 times bending, while still providing adequate mechanical protection. Higher pressures result in significantly larger changes in electrical properties both while encapsulating and under bending stress. Therefore, for applications prioritizing both flexibility and electrical stability, encapsulation pressures in the 200-400 psi range seem to offer the best overall performance. Prior studies have not explored the bending of encapsulated graphene, marking a significant first in our research. This pioneering effort opens new avenues for the application of graphene in flexible electronics. While there is no existing research on how bending cycles affect electrical resistance changes in encapsulated graphene, as mentioned before in this chapter previous studies have focused extensively on resistance after encapsulation. For example, the sheet

resistance of bare graphene (BG) increased dramatically upon encapsulation, rising from 1.5 $k\Omega$/sq to 15.9 $k\Omega$/sq with thermal evaporation (TE) SiO2, and from 3.1 $k\Omega$/sq to 341.4 $k\Omega$/sq using pulsed electron deposition (PED) SiO2. These significant changes highlight the profound impact of encapsulation methods on graphene's electrical properties. [67] In parallel, an examination of Laser Induced Graphene (LIG) composites reveals that laminating LIG with various materials substantially affects their resistance. In this study, resistance changes were noted from 0.13 $k\Omega$/sq to 0.44 $k\Omega$/sq for LDPE/LIG/LDPE, to 0.47 $k\Omega$/sq for both LDPE/LIG/HDPE and Duct Tape/LIG/LDPE, to 0.57 $k\Omega$/sq for LDPE/LIG/Cheesecloth, to 0.68 $k\Omega$/sq for LDPE/LIG/Kimwipe, and to 0.76 $k\Omega$/sq for LDPE/LIG Pattern/LDPE, demonstrating at least a 238% increase in resistance for the LDPE/LIG/LDPE composite. [43]

Comparatively, the changes in resistance after three bending cycles in our work are notably lower than those observed after encapsulation.

Furthermore, bending tests were conducted to evaluate the mechanical robustness of non-encapsulated LIG under repeated bending cycles. The resistance of non-encapsulated LIG was measured before and after three bending cycles at varying bending radii of 25 mm, 35 mm, and 45 mm. The measurements were performed using a digital multimeter, and the percentage increase in resistance was calculated to quantify the impact of mechanical strain on the electrical performance of the LIG samples.

The results, as shown in 4.2 indicated a significant increase in resistance after bending, particularly for smaller bending radii. At a bending radius of 25 mm, the resistance increased by an average of 518%, while at 35 mm, the increase was approximately 461%, and at 45 mm, it was 343%.

Table 4.2: Change in resistance of non-encapsulated LIG after three bending cycles with 25mm, 35mm, and 45mm bending radii

Resistance Before Bending ()	**bending radius (mm)**	**Resistance After Bending ()**	**% Increase**	**Average % Increase**
34.1	25	243.5	614%	518%
38.0	25	198.6	423%	518%
42.2	25	259.0	517%	518%
43.3	35	188.5	335%	461%
44.1	35	234.6	432%	461%
32.6	35	229.2	616%	461%
32.7	45	172.7	428%	343%
37.2	45	123.4	232%	343%
43.1	45	202.5	370%	343%

These findings reveal a clear inverse relationship between the bending radius and the degree of resistance increase, with smaller bending radii inducing greater mechanical strain and leading to more pronounced changes in resistance. The substantial increase in resistance highlights the susceptibility of non-encapsulated LIG to structural and electrical degradation under repeated bending cycles.

In comparison, encapsulated LIG samples demonstrated significantly enhanced mechanical robustness under similar testing conditions. Encapsulation effectively mitigated the resistance increase observed during bending, with encapsulated samples showing only a modest resistance increase, typically in the range of 50–100%, even at smaller bending radii. This stark difference underscores the critical role of encapsulation in preserving the structural integrity of LIG under

mechanical stress. Encapsulated LIG exhibits superior performance in bending tests, making it far more suitable for applications in flexible and wearable electronics where mechanical deformation is unavoidable.

These findings emphasize the importance of encapsulation in improving the durability and reliability of LIG-based devices. While non-encapsulated LIG may exhibit promising electrical properties in static conditions, its performance deteriorates significantly when subjected to mechanical deformation. Encapsulation serves as an effective protective measure, ensuring the longevity and stability of LIG under bending stress and enhancing its potential for practical applications in environments that demand mechanical flexibility. This comparison between non-encapsulated and encapsulated LIG highlights the necessity of implementing robust protective measures for LIG to ensure consistent performance in real-world applications.

4.4 Durability of Encapsulated LIG in Moist Environments

To assess the durability of LIG when exposed to moisture, we conducted an experiment where ten LIG samples encapsulated at 80 psi were fully immersed in a beaker of water for 24 hours. This test aimed to simulate extended exposure to moist conditions and evaluate the impact on the material's electrical resistance. Prior to immersion, the initial resistance of each sample was recorded, and subsequent measurements were taken immediately after removal from the water. The results, detailed in Table 4.3, demonstrate the encapsulated LIG's resistance stability when subjected to moisture. Fig. 4.4 illustrates the setup of the experiment, showing a sample submerged in the beaker. The experiment aimed to assess the impact of moisture on the electrical resistance of

Table 4.3: Resistance of encapsulated LIG before and after 24-hour water immersion

Encapsulated LIG resistance before immersion (ohm)	**Encapsulated LIG Resistance after immersion (ohm)**	**Percent Increase (%)**
42.1	42.6	1.2%
39.5	39.6	0.3%
40.2	40.9	1.7%
41.4	42.0	1.4%
46.8	47.0	0.4%
38.6	38.9	0.7%
45.6	46.1	1.1%
43.6	44.3	1.6%
45.4	45.6	1.1%
39.7	39.9	0.5%

LIG samples encapsulated at 80 psi. After 24 hours of immersion in water, the resistance of the encapsulated LIG samples showed a minimal increase, indicating a high level of durability against moisture. The results are promising as they demonstrate the LIG's ability to maintain electrical properties in a wet environment, which is critical for applications in harsh or outdoor conditions. The maximum percent increase observed was 1.7%, with most samples showing changes between 0.4% to 1.4%, suggesting a uniform and stable behavior under moisture exposure.

We conducted another test with non-encapsulated LIG to establish a baseline for comparison. to do so, we performed identical moisture tests on non-encapsulated LIG samples. As shown in the Table 4.4, the results show that the resistance increased by up to 3.7%, whereas the resistance increase for encapsulated LIG was limited to 1.7%. These findings demonstrate that our encapsulation method is effective in improving the moisture resistance of LIG, despite the initial resistance change being minimal.

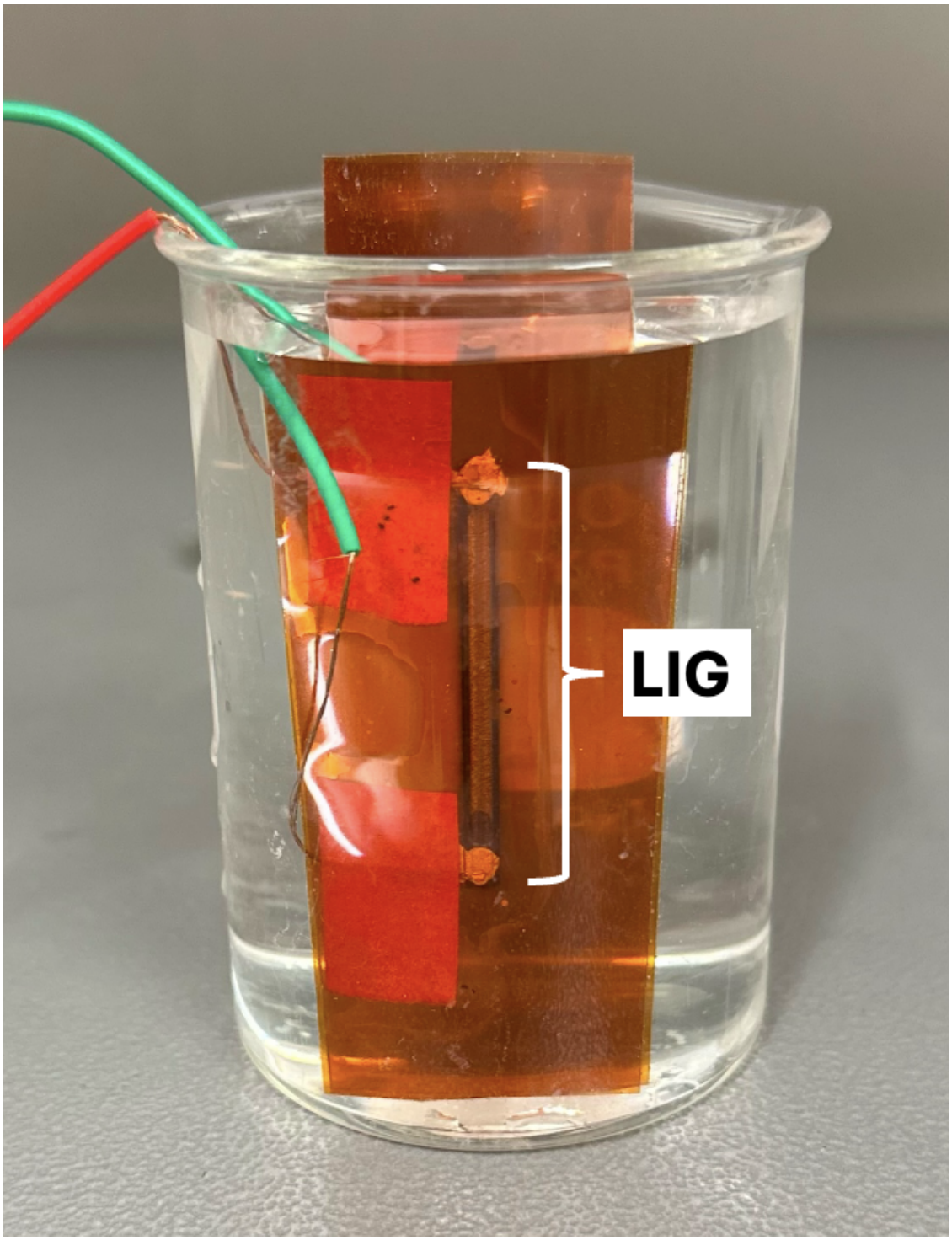

Figure 4.4: Experimental setup showing an encapsulated LIG sample fully immersed in water for durability testing, with contacts and wires connected to measure resistance changes.

Table 4.4: Resistance of non-encapsulated LIG before and after 24-hour water immersion

Non-encapsulated LIG resistance before immersion (ohm)	**Non-encapsulated LIG Resistance after immersion (ohm)**	**Percent Increase (%)**
38.9	39.6	1.8%
34.5	34.7	0.5%
42.4	43.2	1.8%
40.9	41.8	2.2%
35.0	36.3	3.7%

To evaluate the effectiveness of the encapsulation process on moisture resistance, we conducted a statistical analysis comparing resistance changes in encapsulated (n=10) and non-encapsulated (n=5) LIG samples after water exposure. The resistance of each sample was measured before and after immersion in water. A two-sample t-test was performed to determine statistical significance between the two groups' resistance changes. The analysis was conducted using standard statistical methods, with percent change in resistance as the primary metric. Standard error was calculated for both groups to account for measurement uncertainty and sample variation.

As shown in the Fig. 4.5 in the statistical analysis was performed to evaluate the effectiveness of encapsulation on water resistance. A two-sample t-test comparing the resistance changes after water exposure showed that encapsulated samples exhibited significantly better stability (1.0 ± 0.47% increase) compared to non-encapsulated samples (2.0 ± 0.58% increase) ($p < 0.05$). This demonstrates that the encapsulation process effectively improves the water resistance of LIG samples.

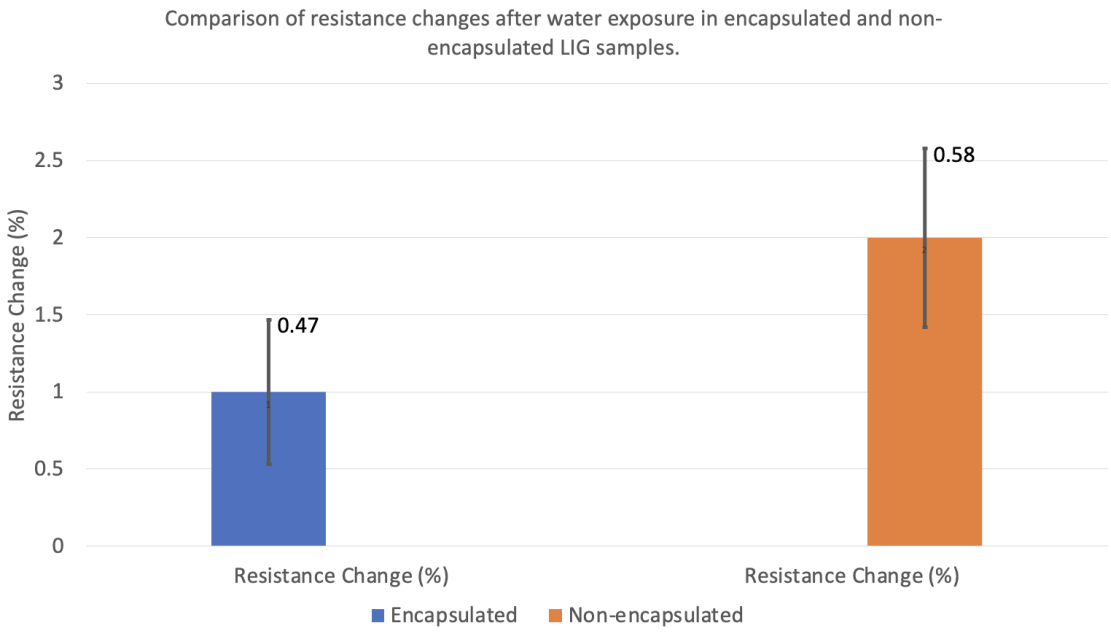

Figure 4.5: Comparison of resistance changes after water exposure in encapsulated and non-encapsulated LIG samples. Error bars represent standard error (n=10 for encapsulated, n=5 for non-encapsulated, $p < 0.05$).

Chapter 5

Structural and Morphological Characterization

5.1 Raman Spectroscopy Analysis

Raman spectroscopy provides crucial insights into the structural characteristics and quality of our LIG samples, allowing us to examine the effects of varying encapsulation pressures on the graphene structure at the molecular level.

The Raman spectroscopy analysis of our LIG samples (Fig. 5.1) reveals significant structural changes induced by varying encapsulation pressures. The unencapsulated sample exhibits characteristics of few-layer graphene, with an I(D)/I(G) ratio of 0.862 indicating the presence of defects and flake edges, and an I(2D)/I(G) ratio of 0.721 suggesting a graphene-like structure with multiple layers. The full width at half maximum (FWHM) of the 2D peak (67.5 cm^{-1}) further confirms

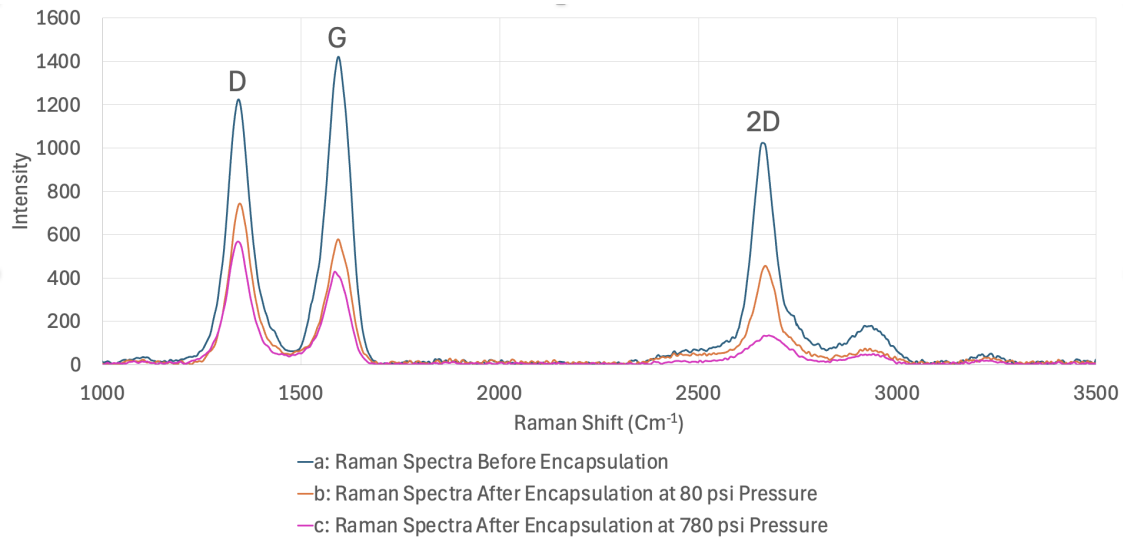

Figure 5.1: Raman spectra of our LIG samples. a) before encapsulation, b) after encapsulation with 80 psi pressure, c) after encapsulation with 780 psi pressure. The prominent peaks are the D peak near 1350 cm^{-1}, the G peak near 1600 cm^{-1}, and the 2D peak near 2700 cm^{-1}.

the few-layer nature of the graphene. The relatively symmetric shape of the 2D peak is similar to observations for single layer graphene or turbostratic stacking of relatively weakly coupled graphene planes. [68–71] Upon encapsulation at 80 psi, we observe an increase in the I(D)/I(G) ratio to 1.286, indicating the introduction of additional defects and/or structural deformation. However, the slight increase in I(2D)/I(G) ratio to 0.789 and similar FWHM values suggest that the overall graphene-like character is maintained with minimal additional layer coupling. The most dramatic changes occur with encapsulation at 780 psi, where the I(D)/I(G) ratio further increases to 1.323, signifying a higher defect density. Concurrently, the I(2D)/I(G) ratio drops significantly to 0.314, and the FWHM(2D) broadens to 125 cm^{-1}, indicating a substantial shift towards a more disordered structure with broader distributions in strain.

These progressive changes in peak ratios and widths across the pressure range provide crucial insights into the structural evolution of our LIG samples. The data suggests that while low-pressure encapsulation introduces some defects, it largely preserves the graphene-like character. In contrast, high-pressure encapsulation leads to more substantial alterations, including increased defects, stronger layer coupling, and a transition towards a more disordered structure.

Raman spectroscopy analysis revealed characteristic features aligned with literature findings for graphene structures. The non-encapsulated LIG showed an I_{2D}/I_G ratio of 0.721, comparable to literature values (~0.8) indicative of few-layer graphene [72, 73], further supported by an I_D/I_G ratio of 0.862. The FWHM of the 2D peak showed progressive broadening from 67.5 cm^{-1} in non-encapsulated samples to 125 cm^{-1} at high encapsulation pressures, consistent with literature observations of compressive strain effects in graphene structures [74–76]. The structural evolution under increasing encapsulation pressure was evidenced by changes in crystallinity markers, where higher pressure samples exhibited increased I_D/I_G ratios (1.323 at 780 psi) and decreased I_{2D}/I_G ratios (0.314), deviating from the metrics associated with highly crystalline graphene ($I_{2D}/I_G \approx 1$) [77, 78]. These Raman metrics collectively demonstrate pressure-dependent structural modifications, transitioning from few-layer graphene characteristics to more disordered, multilayered configurations under higher encapsulation pressures.

These findings have important implications for optimizing the encapsulation process, indicating that lower pressures are preferable for maintaining the desirable properties of graphene in LIG samples. The stability of FWHM values for D and G peaks across all samples suggests that the basic graphitic structure is maintained even under high pressure, but the changes in peak intensities

and 2D peak width reveal significant alterations in interlayer interactions, strain and defect density. This comprehensive analysis provides valuable guidance for tailoring the encapsulation process to achieve desired structural properties in LIG for various applications.

5.2 SEM Analysis

SEM provides a powerful tool for visualizing the microstructural changes in our encapsulated LIG samples subjected to various mechanical stresses. This section presents a detailed analysis of the SEM observations, offering crucial insights into the morphological evolution of LIG structures under different encapsulation pressures.

The unencapsulated LIG, shown in Fig. 5.2, exhibits a highly porous, three-dimensional network structure characteristic of LIG. At lower magnifications, we observe an arrangement of interconnected pores with varying sizes, ranging from a few micrometers to tens of micrometers in diameter. The higher magnification image reveals the intricate nature of the graphene sheets forming the walls of these pores, with thin, wrinkled sheets creating a complex, interconnected network. This structure provides the large surface area and high conductivity typical of LIG materials. Upon encapsulation at 80 psi, as observed in Fig. 5.3, there are no noticeable changes in the microstructure of the LIG sample at any magnification level (200 μm, 100 μm, and 2 μm), when comparing before and after encapsulation. This consistency across all magnifications is in confirmation with the minimal changes in electrical resistance noted after encapsulation, as evidenced in Fig. 4.1, indicating that low-pressure encapsulation preserves the original structural and electrical properties of the LIG

The most dramatic structural changes are observed in the LIG samples encapsulated at 780 psi,

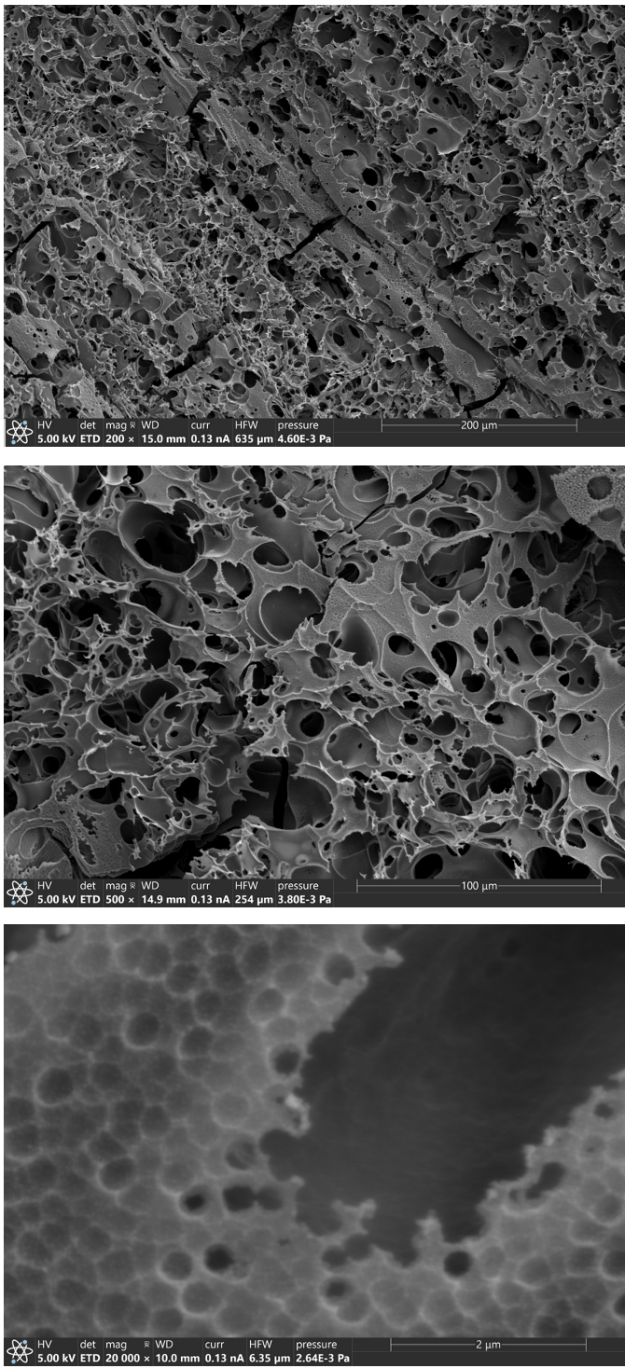

Figure 5.2: SEM images of LIG sample before encapsulation at different magnifications.

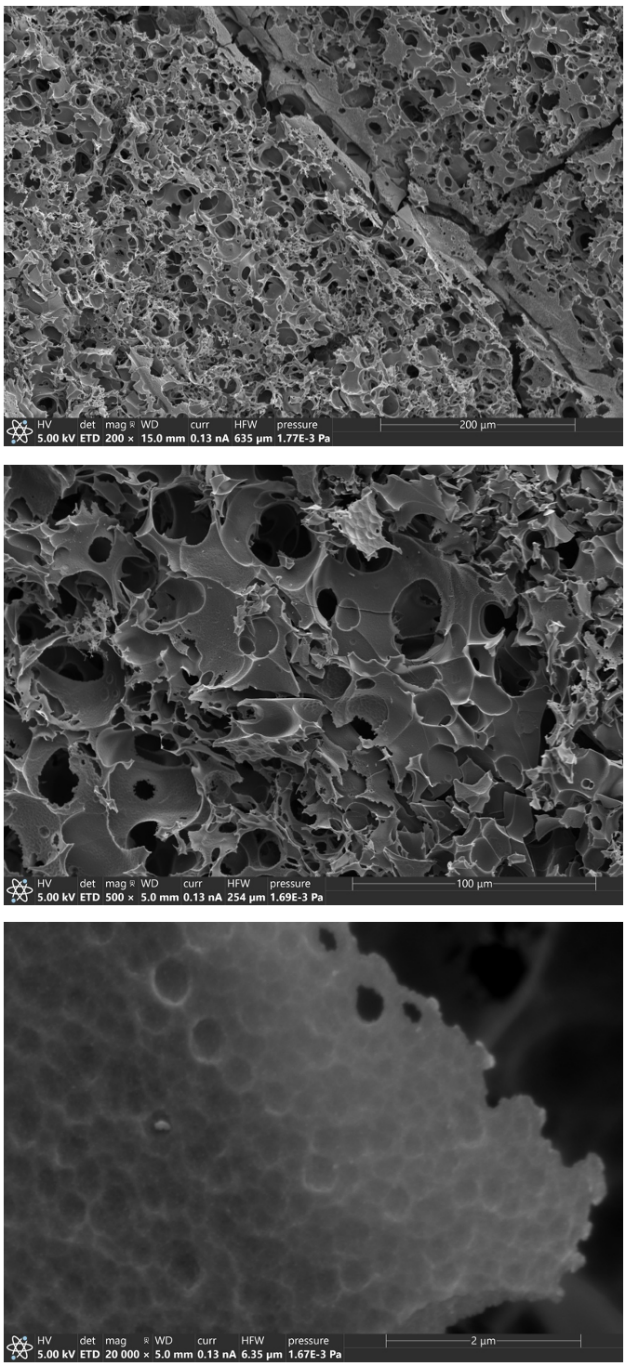

Figure 5.3: SEM images of LIG sample after encapsulation with 80 psi pressure at different magnifications.

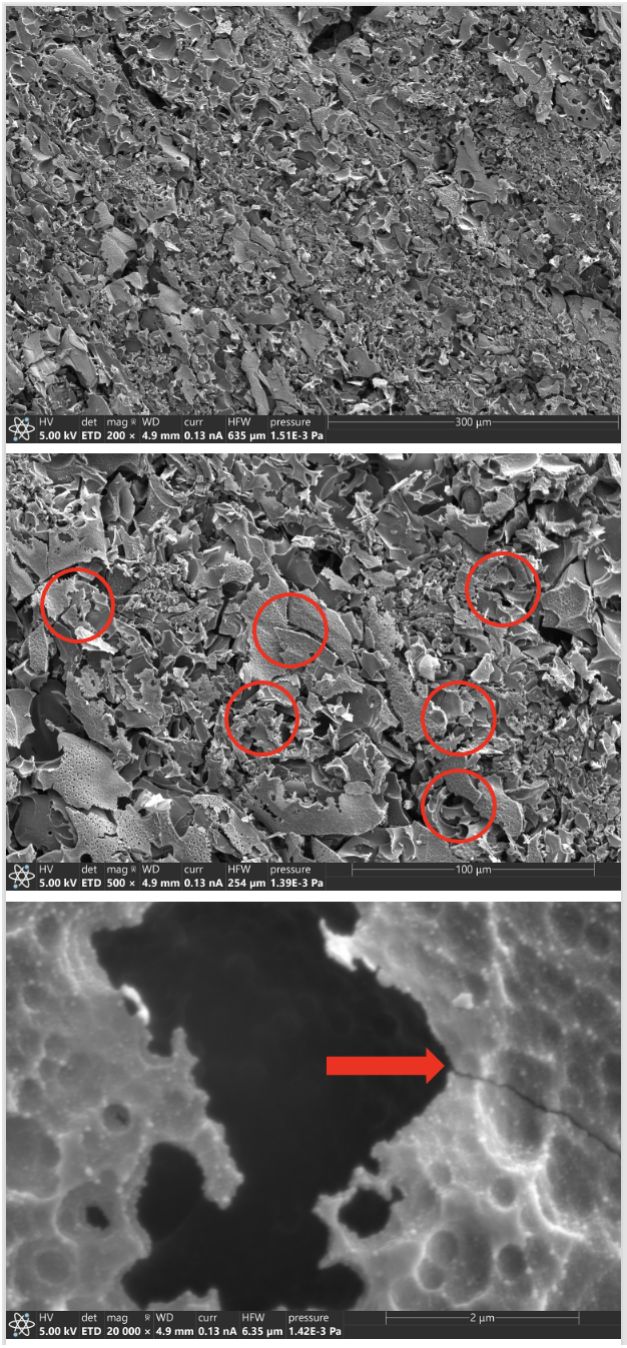

Figure 5.4: SEM images of LIG sample after encapsulation with 780 psi pressure at different magnifications.

as depicted in Fig. 5.4. At this high pressure, the porous network structure has undergone significant compression and partial collapse. The lower magnification images reveal a much denser structure with smaller, less distinct pores. The graphene sheets appear to have been forced closer together, resulting in a more compact, less three-dimensional structure. The highest magnification image shows evidence of sheet stacking (layering of graphene sheets on top of each other), as shown in the red circles, and fracture of graphene layers, as shown in 2 μm magnification with red arrow. This structural evolution suggests a transition towards a more disordered and strained material, confirming the Raman spectroscopy findings of increased structural perturbation and a shift away from the graphene-like character at higher encapsulation pressures.

These SEM observations provide crucial visual evidence of the pressure-induced structural changes in LIG. They demonstrate that while low-pressure encapsulation largely preserves the desirable porous network structure of LIG, high-pressure encapsulation leads to significant structural densification and potential loss of the unique properties associated with the three-dimensional graphene network.

Chapter 6

Conclusions

6.1 Summary of Findings

This research presents a novel approach to enhancing the mechanical robustness of laser-induced graphene while preserving its exceptional electrical properties. Our key accomplishment was the development of a facile encapsulation technique using sticky Kapton tape and controlled pressure application, achieving better results than previous attempts. This method proved effective at pressures as low as 80 psi. In terms of electrical performance, our encapsulation method minimized the increase in resistance to just 5% of the LIG's original value at low pressures (80 - 400 psi), a significant improvement over existing techniques which typically result in 200-300% increases in resistance. The initial sheet resistance of approximately 2.2 $\Omega/square$ represents a very low value among values reported for LIG. The encapsulated samples showed remarkable resistance to mechanical stress, with resistance changes limited to 64-75% after three bending cycles at optimal

encapsulation pressures. This stability remained consistent across different bending radii (15-45 mm). Furthermore, water immersion tests demonstrated exceptional environmental durability, with resistance changes limited to 1-5% after 24-hour exposure, indicating effective protection against environmental factors.

6.2 Novel Contributions and Implications

This research makes several contributions to the field of LIG technology. Most notably, it represents the first comprehensive study of in-situ resistance changes during the encapsulation process of LIG, providing unprecedented insights into the structural change under pressure. Through combined Raman spectroscopy and SEM analysis, we established a correlation between applied pressure and structural changes in LIG, demonstrating that lower pressures (80 psi) preserve the desirable porous network structure while providing adequate protection. Our work achieved an optimal balance between mechanical protection and electrical conductivity preservation, addressing a challenge in LIG applications. The implications of these findings extend across various applications in modern electronics. The enhanced mechanical stability while maintaining conductivity makes this material particularly suitable for flexible circuits and displays. The demonstrated water resistance and mechanical durability enable applications in wearable sensors and biomedical devices. Furthermore, the comprehensive protection offered by our encapsulation method opens possibilities for LIG use in challenging environmental conditions, expanding its potential application range significantly.

6.3 Future Research Directions

Looking forward, several promising avenues emerge from this work. Our thermal stability studies demonstrated good performance at 90°C, but investigating behavior at higher temperatures could significantly expand application possibilities. This would require exploring alternative substrate materials with higher temperature tolerance. Additionally, conducting extended cycling tests beyond the current three-cycle limit would provide valuable insights into long-term durability and potential fatigue effects. Research is also needed into effective methods for integrating encapsulated LIG with other electronic components, particularly addressing connection points and interfaces. The scaling of our encapsulation method to larger areas and different LIG patterns remains crucial for industrial applications. Moreover, understanding the behavior of encapsulated LIG under dynamic loading conditions would be essential for applications in flexible electronics and wearable devices. The novel methodology and findings presented in this thesis provide a foundation for future developments in flexible electronics and sensing applications using LIG. By addressing the fundamental challenge of maintaining electrical properties while enhancing mechanical stability, this work contributes significantly to advancing the practical implementation of LIG-based technologies. The simplicity and effectiveness of our approach, combined with the characterization of material properties under various conditions, opens new possibilities for the integration of LIG in next-generation electronic devices.

References

[1] Anwar A, Mohammed B S, Wahab M A and Liew M 2020 *Developments in the Built Environment* **1** 100002

[2] Rao C, Biswas K, Subrahmanyam K and Govindaraj A 2009 *Journal of Materials Chemistry* **19** 2457–2469

[3] Geim A K and Novoselov K S 2007 *Nature materials* **6** 183–191

[4] Cooper D R, D'Anjou B, Ghattamaneni N, Harack B, Hilke M, Horth A, Majlis N, Massicotte M, Vandsburger L, Whiteway E *et al.* 2012 *International Scholarly Research Notices* **2012** 501686

[5] Novoselov K S, Geim A K, Morozov S V, Jiang D e, Zhang Y, Dubonos S V, Grigorieva I V and Firsov A A 2004 *science* **306** 666–669

[6] Ye R, James D K and Tour J M 2019 *Advanced Materials* **31** 1803621

[7] Xu Y, Sheng K, Li C and Shi G 2010 *ACS nano* **4** 4324–4330

[8] Stoller M D, Park S, Zhu Y, An J and Ruoff R S 2008 *Nano letters* **8** 3498–3502

[9] Mayorov A S, Gorbachev R V, Morozov S V, Britnell L, Jalil R, Ponomarenko L A, Blake P, Novoselov K S, Watanabe K, Taniguchi T *et al.* 2011 *Nano letters* **11** 2396–2399

[10] Balandin A A 2011 *Nature materials* **10** 569–581

[11] Balandin A A, Ghosh S, Bao W, Calizo I, Teweldebrhan D, Miao F and Lau C N 2008 *Nano letters* **8** 902–907

[12] Geim A K 2009 *science* **324** 1530–1534

[13] Olenych I B, Aksimentyeva O I, Monastyrskii L S, Horbenko Y Y, Partyka M V, Luchechko A P and Yarytska L I 2016 *Nanoscale research letters* **11** 1–7

[14] Ye R, James D K and Tour J M 2018 *Accounts of chemical research* **51** 1609–1620

[15] Sun Z, Fang S and Hu Y H 2020 *Chemical Reviews* **120** 10336–10453

[16] Zhang L and Shi G 2011 *The Journal of Physical Chemistry C* **115** 17206–17212

[17] Chen W and Yan L 2011 *Nanoscale* **3** 3132–3137

[18] Sheng K x, Xu Y x, Chun L and Shi G q 2011 *New Carbon Materials* **26** 9–15

[19] Sohn K, Na Y J, Chang H, Roh K M, Jang H D and Huang J 2012 *Chemical communications* **48** 5968–5970

[20] Choi B G, Yang M, Hong W H, Choi J W and Huh Y S 2012 *ACS nano* **6** 4020–4028

[21] Kumar S, McEvoy N, Kim H Y, Lee K, Peltekis N, Rezvani E, Nolan H, Weidlich A, Daly R and Duesberg G S 2011 *physica status solidi (b)* **248** 2604–2608

[22] Wang X, You H, Liu F, Li M, Wan L, Li S, Li Q, Xu Y, Tian R, Yu Z *et al.* 2009 *Chemical Vapor Deposition* **15** 53–56

[23] Guo Y, Zhang C, Chen Y and Nie Z 2022 *Nanomaterials* **12** 2336

[24] Lin J, Peng Z, Liu Y, Ruiz-Zepeda F, Ye R, Samuel E L, Yacaman M J, Yakobson B I and Tour J M 2014 *Nature communications* **5** 5714

[25] Dong Z, He Q, Shen D, Gong Z, Zhang D, Zhang W, Ono T and Jiang Y 2023 *Microsystems & Nanoengineering* **9** 31

[26] Le T S D, Phan H P, Kwon S, Park S, Jung Y, Min J, Chun B J, Yoon H, Ko S H, Kim S W *et al.* 2022 *Advanced Functional Materials* **32** 2205158

[27] Sharaf S M 2020 Smart conductive textile *Advances in functional and protective textiles* (Elsevier) pp 141–167

[28] Zhang S, Ukrainczyk N, Zaoui A and Koenders E 2024 *Construction and Building Materials* **411** 134536

[29] Stanford M G, Yang K, Chyan Y, Kittrell C and Tour J M 2019 *ACS nano* **13** 3474–3482

[30] Nazeri M, Ghalamboran M and Grau G 2023 *Advanced Materials Technologies* **8** 2300188

[31] Chyan Y, Ye R, Li Y, Singh S P, Arnusch C J and Tour J M 2018 *ACS nano* **12** 2176–2183

[32] Ye R, Chyan Y, Zhang J, Li Y, Han X, Kittrell C and Tour J M 2017 *Advanced Materials* **29** 1702211

[33] Peng Z, Lin J, Ye R, Samuel E L and Tour J M 2015 *ACS applied materials & interfaces* **7** 3414–3419

[34] Ma W, Zhu J, Wang Z, Song W and Cao G 2020 *Materials Today Energy* **18** 100569

[35] Wan Z, Nguyen N T, Gao Y and Li Q 2020 *Sustainable Materials and Technologies* **25** e00205

[36] Stanford M G, Li J T, Chyan Y, Wang Z, Wang W and Tour J M 2019 *ACS nano* **13** 7166–7174

[37] Kulyk B, Silva B F, Carvalho A F, Silvestre S, Fernandes A J, Martins R, Fortunato E and Costa F M 2021 *ACS Applied Materials & Interfaces* **13** 10210–10221

[38] Vivaldi F M, Dallinger A, Bonini A, Poma N, Sembranti L, Biagini D, Salvo P, Greco F and Di Francesco F 2021 *ACS Applied Materials & Interfaces* **13** 30245–30260

[39] Wang H, Zhao Z, Liu P and Guo X 2022 *Biosensors* **12** 55

[40] Luong D X, Yang K, Yoon J, Singh S P, Wang T, Arnusch C J and Tour J M 2019 *ACS nano* **13** 2579–2586

[41] Usman M, Jafry A T, Abbas A, Hussain G and Abbas N 2023 *Thin Solid Films* **780** 139979

[42] Sinha K 2020

[43] Li J T, Stanford M G, Chen W, Presutti S E and Tour J M 2020 *ACS nano* **14** 7911–7919

[44] Tehrani F, Beltrán-Gastélum M, Sheth K, Karajic A, Yin L, Kumar R, Soto F, Kim J, Wang J, Barton S *et al.* 2019 *Advanced Materials Technologies* **4** 1900162

[45] Cao L, Zhu S, Pan B, Dai X, Zhao W, Liu Y, Xie W, Kuang Y and Liu X 2020 *Carbon* **163** 85–94

[46] Melios C, Giusca C E, Panchal V and Kazakova O 2018 *2D Materials* **5** 022001

[47] Shaikh S F and Hussain M M 2020 *Applied Physics Letters* **117**

[48] Biswas R K, McGlynn P, O'Connor G M and Scully P 2023 *Materials Letters* **343** 134362

[49] Jeong S, Kwon Y, Park C, Ito Y, Park J, Hwang M S, Chung J and Sugita N 2024 *Nano Energy* **126** 109663

[50] Lamberti A, Perrucci F, Caprioli M, Serrapede M, Fontana M, Bianco S, Ferrero S and Tresso E 2017 *Nanotechnology* **28** 174002

[51] King A A, Davies B R, Noorbehesht N, Newman P, Church T L, Harris A T, Razal J M and Minett A I 2016 *Scientific reports* **6** 1–6

[52] Ferrari A C and Basko D M 2013 *Nature nanotechnology* **8** 235–246

[53] Beams R, Cançado L G and Novotny L 2015 *Journal of Physics: Condensed Matter* **27** 083002

[54] Dresselhaus M, Jorio A, Souza Filho A and Saito R 2010 *Philosophical Transactions of the Royal Society A: Mathematical, Physical and Engineering Sciences* **368** 5355–5377

[55] Zhang S, Wang J, Li Z, Zhao R, Tong L, Liu Z, Zhang J and Liu Z 2016 *The Journal of Physical Chemistry C* **120** 10605–10613

[56] Ni Z H, Yu T, Lu Y H, Wang Y Y, Feng Y P and Shen Z X 2008 *ACS nano* **2** 2301–2305

[57] Wu J B, Lin M L, Cong X, Liu H N and Tan P H 2018 *Chemical Society Reviews* **47** 1822–1873

[58] Wang Y, Yao M, Chen Y, Dong J, Yang X, Du M, Liu R, Liu H, Li Y and Liu B 2018 *Applied Physics Letters* **113**

[59] Kim S, Park S, Kim H, Jang G, Park D, Park J Y, Lee S and Ahn Y 2016 *Applied Physics Letters* **108**

[60] Koehler F M, Jacobsen A, Ihn T, Ensslin K and Stark W J 2012 *Nanoscale* **4** 3781–3785

[61] Tavakkoli Gilavan M, Rahman M S, Minhas-Khan A, Nambi S and Grau G 2021 *ACS Applied Electronic Materials* **3** 3867–3875

[62] Beckham J L, Li J T, Stanford M G, Chen W, McHugh E A, Advincula P A, Wyss K M, Chyan Y, Boldman W L, Rack P D *et al.* 2021 *ACS nano* **15** 8976–8983

[63] Jiao L, Chua Z Y, Moon S K, Song J, Bi G, Zheng H, Lee B and Koo J 2019 *Nanomaterials* **9** 90

[64] Zhang Z, Song M, Hao J, Wu K, Li C and Hu C 2018 *Carbon* **127** 287–296

[65] Le H, Minhas-Khan A, Nambi S, Grau G, Shen W and Wu D 2023 *Flexible and Printed Electronics* **8** 035013

[66] Minhas-Khan A, Nambi S and Grau G 2021 *Carbon* **181** 310–322

[67] Kalkan S B, Yanilmaz A and Çelebi C 2019 *Journal of Vacuum Science & Technology A* **37**

[68] Xueshen W, Jinjin L, Qing Z, Yuan Z and Mengke Z 2013 *Journal of Nanomaterials* **2013** 101765

[69] Wei C, Negishi R, Ogawa Y, Akabori M, Taniyasu Y and Kobayashi Y 2019 *Japanese Journal of Applied Physics* **58** SIIB04

[70] Gupta N, Walia S, Mogera U and Kulkarni G U 2020 *The Journal of Physical Chemistry Letters* **11** 2797–2803

[71] Stubrov Y, Nikolenko A, Strelchuk V, Nedilko S and Chornii V 2017 *Nanoscale research letters* **12** 1–6

[72] Duy L X, Peng Z, Li Y, Zhang J, Ji Y and Tour J M 2018 *Carbon* **126** 472–479

[73] Sun Z, Raji A R O, Zhu Y, Xiang C, Yan Z, Kittrell C, Samuel E and Tour J M 2012 *Acs Nano* **6** 9790–9796

[74] Sokolov D A, Shepperd K R and Orlando T M 2010 *The Journal of Physical Chemistry Letters* **1** 2633–2636

[75] Ferralis N, Maboudian R and Carraro C 2008 *Physical review letters* **101** 156801

[76] Sharma N, Oh D, Abernathy H, Liu M, First P N and Orlando T M 2010 *Surface science* **604** 84–88

[77] de la Roche J, López-Cifuentes I and Jaramillo-Botero A 2023 *Carbon Letters* **33** 587–595

[78] Li X, Sagar R U R, Zhong L, Liu Y, Hui D and Zhang M 2019 *Materials Letters* **248** 43–47